浙江大学

本科生毕业论文（设计）

文献综述和开题报告

姓名与学号 张凯瑜 3180101377

指导教师 郑旭东

年级与专业 2018级飞行器设计与工程

所在学院 航空航天学院

一、题目：MEMS 四质量块微陀螺仪结构设计

二、指导教师对文献综述、开题报告、外文翻译的具体要求

1、查阅与毕业论文（设计）相关的文献不少于 15 篇（其中外文文献不少于 3 篇），译文（译文可作为文献的一部分）和文献综述（包括国内外现状、研究方向、进展情况、存在问题、参考依据）要求字数各 3000 字以上，文献综述内容要切题。

2、开题报告(包括课题意义、背景及可行性分析、调研报告、研究方案、实施计划、预期结果等)要求字数 4000 字以上。

3、对开题答辩，答辩的时间不少于 15 分钟（含提问），学生陈述时间为 8-10 分钟。

指导教师（签名）_____

年　　月　　日

目录

一、文献综述

1、微陀螺仪概述

微机械陀螺是一种测试角速度或角位移的惯性传感器,微机械陀螺基于硅微机械加工技术的特点使得其与传统的机械转子陀螺、光学陀螺相比，体积更小、功耗更低且可靠性高、可批量生产，在军事、消费电子等领域有着广泛的应用前景，因此微机械陀螺一直是各研究机构的研究热点。

1.1 微机械陀螺的主要性能指标

微陀螺仪的性能[1]决定了其导航定位的精准性，主要根据以下几个参数来评估，根据其数值的差异可以划分为速率级、战术级和惯导级三个等级，其具体的划分标准如表1-1所示。

参数	速率级	战术级	惯导级
标度因子非线性度/%FS	0.1~1	0.001~0.1	<0.001
零偏稳定性/deg/h	10~1000	0.01~10	<0.01
角度随机游走系数/deg/√h	>0.5	0.001~0.5	<0.001
动态范围/deg/s	50~1000	>500	>400
带宽/Hz	>70	~100	~100

表 1-1 微陀螺仪性能等级[1]

（一）标度因子非线性度

标度因子的值表示的是外界有角速度输入的状态下陀螺仪输出与输入曲线的斜率，而采用最小二乘法进行拟合的曲线与输出输入曲线的偏离程度用标度因子非线性度来表示，这也是陀螺仪性能等级的评估指标。

（二）零偏稳定性

由于制造缺陷以及电路噪声等因素，微陀螺仪在无外界输入角速度的情况下也会有一定的输出，输出过程是随机的，其均值对应的外界输入角速度即为零偏。零偏稳定性则是指随机输出数据的标准差所等效对应的外界输入角速度，表示的是输出数据点围绕零偏的波动幅度。

（三）角度随机游走系数

同零偏稳定性一样，角度随机游走系数也是反映零输入条件下噪声干扰的参数，是指一段时间内由白噪声引起的随机输出误差，可以通过艾伦方差曲线进行表征，也是陀螺仪重要的性能指标。

（四）动态范围

陀螺仪在相反两个方向上可以敏感到的最大外界输入角速度的值称为该陀螺仪的量程，在大多数文献资料中动态范围定义为量程与阈值的比值，反映的是陀螺仪对外界转动的敏感程度。

（五）带宽

对带宽的定义是陀螺仪实际可以敏感到的角速度的最大与最小频率之差，反映的是陀螺仪响应外界变化的动态能力。对于开环控制电路来说，带宽即为振幅响应下的3dB频段;而对于闭环控制方式的电路，带宽可以表示为低通滤波器的截止频率。

综上所述，提高微机械陀螺的指标是MEMS陀螺的永恒追求，微机械陀螺在工作过程中会受到环境因素的影响，包括温度、加速度冲击等，这就制约了微机械陀螺实际工程应用的范围。因此，微机械陀螺的设计不仅要求性能指标优秀，更需要增强环境适应性，本项目设计的基于SOG的结构解耦四质量块微陀螺仪环境适应性优秀，符合MEMS陀螺未来的发展趋势。

2、国内外研究现状及总结

MEMS陀螺仪和其他陀螺（例如光纤陀螺、环形激光陀螺、半球谐振陀螺和石英陀螺仪）相比具有许多关键的优势：低成本、轻量级、在严酷环境下的可靠性和低功耗。随着人工智能、物联网时代的加速到来，MEMS 陀螺仪越来越得到广泛的应用，渗透到人们工作、生活中的各个方面。手里拿的智能手机，耳朵戴着的TWS耳机，玩的无人机等智能设备都搭载了MEMS陀螺仪。随着半导体技术的发展和智能时代的推进，MEMS陀螺仪已经大规模商用化、民用化，已成为我们日常工作和生活中的一部分。本文所设计的四质量块微陀螺仪属于基于科氏效应的微振动陀螺仪类型，因此本节将着重介绍四质量块的结构型式及其发展概况。

四质量块微陀螺仪属于一种比较新颖的类型，是在音叉陀螺仪结构上改进而来的，主要是为了消除音叉式结构驱动和检测模态的不对称性，实现较低的频率分裂，从而达到更优的性能。目前，四质量块的结构形式在国内外的研究并不多但是其在线振动式微陀螺仪中展现出了很好的发展前景。

2.1 国内外研究现状

2011年，加州大学尔湾分校[2]就对于四质量块陀螺仪特殊的结构优势与速率积分（全角度）的关系进行了研究。与双质量装置类似，四重质量陀螺仪的机械结构，包括四个相同的对称解耦齿、一对用于驱动和检测模式的反相位同步杠杆机构等。四重质量陀螺仪的结构建立在双质量陀螺设计的基础上，可以认为是两个杠杆式双质量陀螺仪与附加的线性弯曲和反相位杠杆机构耦合在一起。四重质量陀螺仪的工作原理如图2.1驱动模式的有限元建模所示。由于器件的对称性，驱动模态和检测模态在90度角上退化和空间定向。

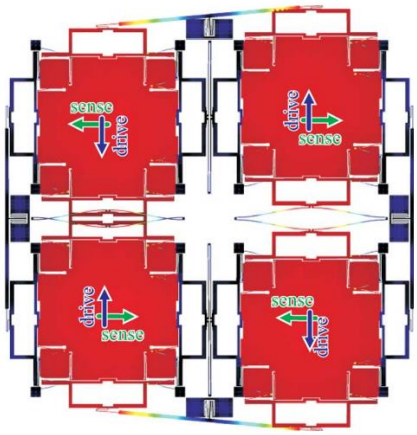

图 2.1 加州大学的四重质量陀螺仪工作方式：退化、反相驱动和检测模式通过机械设计提供完全的动态平衡、低能量损耗以及频率和因数匹配 [2] 。

四重质量陀螺仪保留并扩展了杠杆式双质量设计的结构优势。与传统音叉装置不同，杠杆式四重质量结构提供了沿驱动轴和感应轴的外部振动和机械冲击的真正机械抑制。该装置的结构对称性使得其对制造缺陷和温度引起的频率漂移的鲁棒性有所提高，这是高振动陀螺仪中已知的漂移源。最重要的是，由于其低能量耗散和共振频率和阻尼各向同性的独特组合，四重质量设计有望实现速率积分（全角度）模式。

2012年，加州大学欧文分校的Andrei M. Shkel等[3,4]教授对四质量块进行了理论和工艺的研究。Q因子从最初的31万提升到2016年的170万。加入吸气剂并真空封装，静置一年之后，在微托尔级的真空度下获得了超过2百万的品质因数，零偏稳定性和角度随机游走系数分别达到了 0.09deg/h和0.015deg/h，显示了其具备达到惯导级性能的潜力。

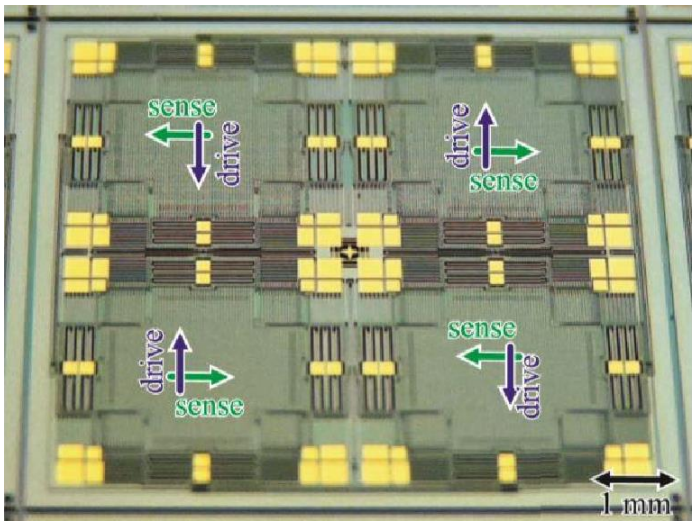

图2.2 加州大学的四质量块微陀螺仪[3]

在2014年，加州大学欧文分校的Andrei M. Shkel[5,6,7]等教授又报道了一种最新开发的四质量陀螺仪（QMG）——集总结构的MEMS II 级CVG。他们提出科里奥利振动陀螺仪（CVG）可根据谐振器的物理形状和涉及的振动模式的性质分为两类。Ⅰ类MEMS CVG是不对称结构，通常作为高Q因数双质量音叉实现，已显示出低端和中型战术级性能的潜力。然而，该技术似乎已达到其基本限制，偏差不确定性约为10 deg/h。而在Ⅱ类CVG中，通常采用振动棒或轴对称壳体，允许驱动轴或模式角度的任意定位。除了速率测量力再平衡模式外，该独特功能还支持全角度和自校准机械化。

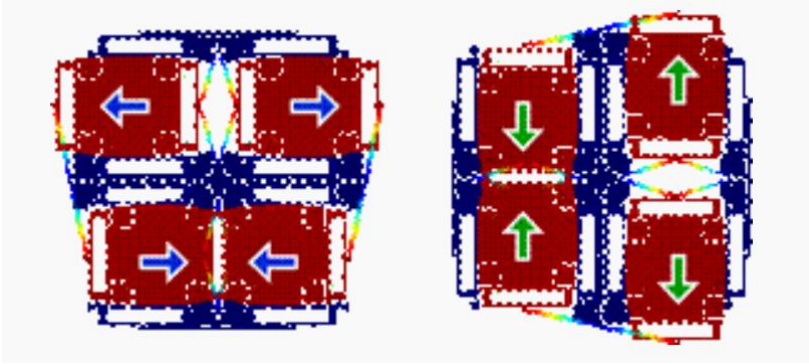

图 2.3 加州大学的四质量陀螺仪谐振器有限元建模，显示了 II 类 CVG 的两个相同振型特征[7]。

其设计的高性能CVG的最佳结构包含模式对称机械结构，结合了非常高的q因子和衰减时间常数，高科里奥利耦合(角增益)，容易的频率调谐能力，以及使用现有硅MEMS工艺的低成本批量制造。QMG换能器，如图2.4所示，由四个对称解耦齿组成，通过内外杠杆机构同步到平衡反相运动，由于消除了锚损和谐振频率和阻尼的各向同性，提供了一种独特的超低能量耗散组合。使用反相位杠杆代替传统的弹簧弯曲，可以实现几个kHz的相对较低的工作频率，同时将寄生同相模式推向更高的刚度，以抑制共模加速度[7]。

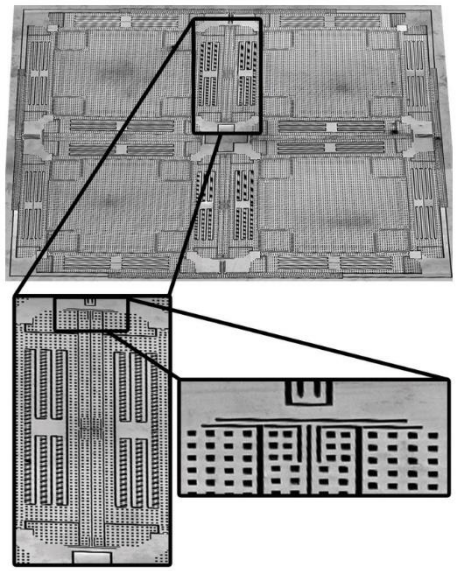

图 2.4 加州大学的显示内杠杆机构设计的扫描电镜图像[7]。

2016年，加州大学伯克利分校Mitchell Kline等[8]提出一种具有非线性补偿的外延封装四轴质量陀螺仪，实验测得其Q值和零漂为85000和 1.6deg/h。

2013年，东南大学夏敦柱教授等[9]报道了一种四质量块形式的四模态匹配三轴硅微陀螺仪，通过双重静电调谐使得四模态的频率分裂最终小于30Hz，热弹性阻尼仿真下得到驱动和检测模态的Q值达到23816和19507。图 2.5(a) 所示该器件主要由 4 个大质量块和 4 个小质量块组成。4 个大质量块绕中心驱动电极四 方对称分布，而 4 个小质量块则如图 2.5(b) 所示分 别嵌在 4 个大质量块中间方孔中，并且由固定在大质量块上的交叉十字多晶硅梁悬挂支撑。如图 2.5(c) 所示，所有的质量块都是由 4 个拐角处的二维的折叠梁支撑，并在 4 个角落处形成锚点。如 图 2.5(d) 所示，该器件共需 5 块掩模板完成，其中 SOI 硅片本身包含了 Handle 层，Buried Oxide 层和器件层。很明显，Handle 层主要作为整个器件的支撑基底，Buried Oxide 层用于区分基底

和器件，器件层才是真正的微惯性器件层，而且我们需要通过 Bosch 工艺刻蚀单晶硅形成深槽。淀积氮化硅层隔离结构层和多晶硅电极层。器件上的多晶硅层采用表面工艺实现，主要作为上电极和正交十字弹性梁。

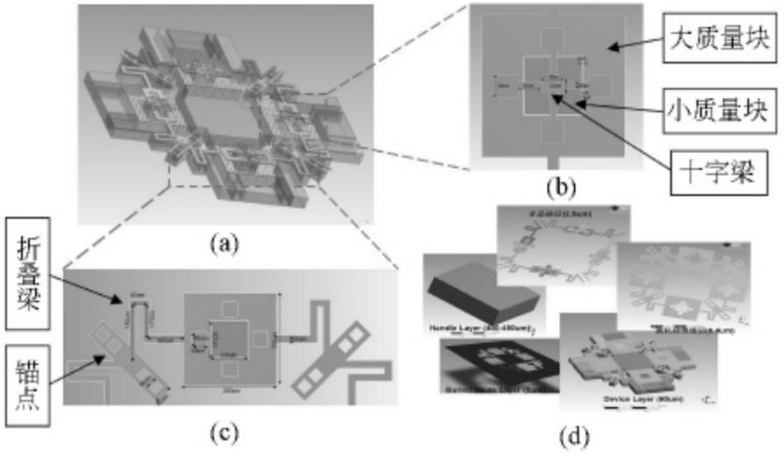

图 2.5 东南大学的三轴陀螺仪示意图[8]

2016年斯坦福大学S.Wisher、P.Shao等[10]提出了一种单驱动工作模式的“高频”谐振三轴音叉陀螺仪。该四质量器件是在一个2x2 mm2真空封装模具上实现的，使用epi-seal工艺，使其成为最小的圆片级封装的三轴陀螺之一。与常规谐振式TFGs相比，谐振频率设计为相对较高(~138 kHz)，允许模式匹配操作的高带宽，并增强了抗冲击和振动。

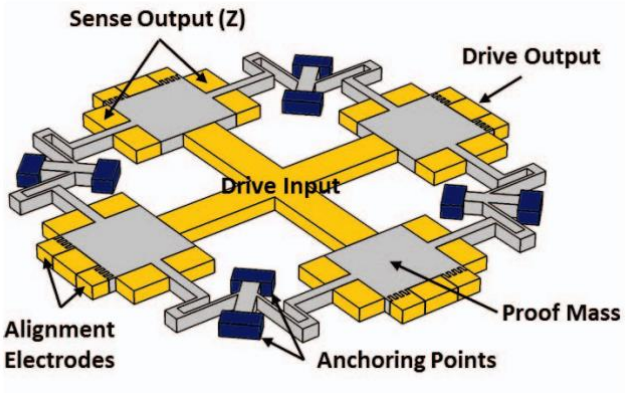

图 2.6 斯坦福大学的单驱动四质量三轴 TFG 示意图[10]

2017年，清华大学张嵘课题组[11]设计并制备了一种中心支撑四质量块陀螺仪,如图2.5所示,四个质量块独立分布,通过折叠梁连接在一中心支撑锚点上。驱动和检测模态的振型类似半球和圆盘多环陀螺仪，因而锚点阻尼相对较小。实验测得其艾伦方差稳定性为0.12deg/h，白噪声水平约为0.72deg/h/$\sqrt{Hz}$，驱动模态下的Q值为8500。

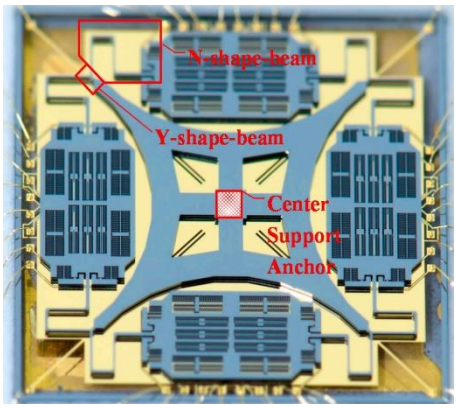

图 2.7 清华大学的中心支撑四质量块微陀螺仪[11]

优化CSQMG的固有频率分配是设计中心支撑四质量块陀螺仪优化的主要目标。清华大学张嵘课题组考虑了含18个变量的蛇形梁的长度和宽度以及参数影响的变化程度，将其固有频率结构分析分为N形梁和Y形梁。为了减轻优化的复杂性，采用控制变量法对这两部分进行分析。并对其进行针对性的独立优化步骤，以消除感模运动和集总质量扭转运动之间的耦合分量。在确定总体结构参数后，对梳齿进行了基于降低机械噪声的优化设计。

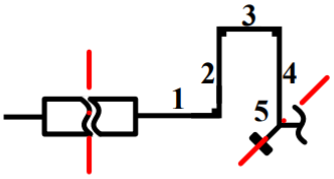

图 2.8 清华大学的 n 型梁优化设计的简化模型[11]。

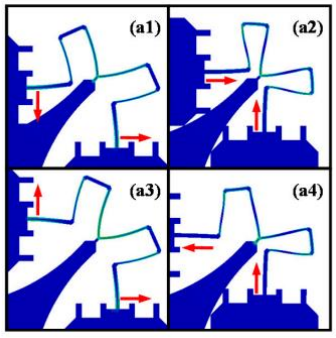

图 2.9 清华大学的 y 形耦合梁在反相位驱动模式下的彩色弹性应变图(a1);反相感应模式(a2);同相驱动方式(a3);和同相检测模式(a4)[11]。

2018年，航空工业西安飞行自动控制研究所的王永等报道了一种环式分布的四质量块微机械陀螺仪[12]，其结构与清华大学类似，为阵列式，品质因数达到20万，其在常温常压下的零漂低于4deg/h，带宽为60Hz。

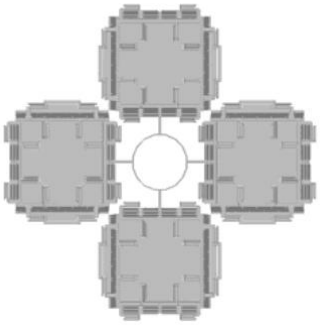

图 2.10 航空工业西安飞行自动控制研究所的环式分布的四质量块陀螺结构简图[12]

2018年，新加坡创新科技署微电子研究所Guoqiang Wu等[13]设计了一种与微吹玻璃半球类似的四质量块陀螺仪，四个质量块通过中心耦合弹簧和四个锥形杠杆耦合在一起，以实现反相位驱动运动的同步，QMG通过机械抑制大大降低了由于加速度和振动而产生的共模信号。驱动和传感方向的动量和扭矩平衡有助于通过锚的超低能量耗散，从而获得高质量因子(Q)和高分辨率。实验测试其艾伦方差零偏稳定性为5.9deg/h，为实现高精度惯性测量单元的高性能陀螺仪设计提供了一种新方法。

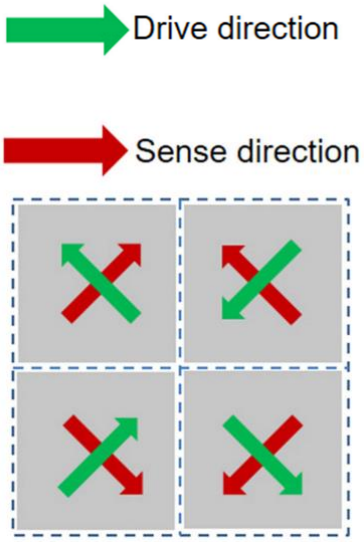

图 2.11 新加坡创新科技署微电子研究所的 QMG 设计：一个对角线方向的两个惯性质量相互远离，而另一个对角线方向的另外两个惯性质量相互靠近[13]。

2.2 总结

如上所述，为四质量块目前几乎全部的国内外研究进展[14]。其中，新加坡创新科技署微电子研究所的四质量块在驱动和检测方向上的动量和扭矩平衡使得锚点处实现超低能耗;加州大学 Shkel 课题组的四质量块由于采用质量块互连

以及超高真空封装技术，其 Q 值几乎逼近热弹性阻尼 Q 值的理论上限;而国内清华大学以及航空工业西安飞行自动控制研究所的四质量块都是阵列式的微半球型式。相对于单质量块陀螺和双质量块陀螺[15]，四质量块陀螺在提高品质因子和抗加速度冲击的方面具有极大的优势，上述的研究对于本文的设计有重大的启迪作用。

3 研究展望

本文以微机械陀螺的四质量块结构为研究对象，通过理论分析，仿真计算等手段，从机械结构层面对微机械陀螺的动力学等效模型进行研究，以解决单质量块陀螺存在的的共模干扰问题，解决两种模态固有频率差异以及检测模态振幅较小问题。本文致力于设计出锚区受力平衡，锚区损耗较小，具有较大的品质因子，能消除冲击扰动影响的基于 SOG 的结构解耦四质量块陀螺，从而实现高精确度、低能量耗散和高共模加速度抑制的成果。

4 参考文献

[1] Jia, Xukai, Ding, et al. Automatic Frequency Tuning Technology for Dual-Mass MEMS Gyroscope Based on a Quadrature Modulation Signal.[J]. Micromachines, 2018.

[2] Trusov A A , Member, IEEE, et al. Low-Dissipation Silicon Tuning Fork Gyroscopes for Rate and Whole Angle Measurements[J]. IEEE Sensors Journal, 2011, 11(11):2763-2770.

[3] Trusov A A , Atikyan G , Rozelle D M , et al.Flat is not dead: Current and futureperformance of Si-MEMS Quad Mass Gyro (QMG) system[C] 2014 IEEE/IONPosition, Location and Navigation Symposium - PLANS 2014.IEEE,2014:252-258.

[4] Trusov A A ,Atikyan G , Rozelle D M , et al.Force rebalance,whole angle,andself-calibration mechanization of silicon MEMSquad mass gyro[C]!I 2014International Symposium on Inertial Sensors and Systems (ISISS).IEEE,2014.

[5] Trusov A A， Atikyan G， Rozelle D M , et al. Force rebalance, whole angle, and self-calibration mechanization of silicon MEMS quad mass gyro[C]// 2014 International Symposium on Inertial Sensors and Systems (ISISS). IEEE, 2014.

[6] Trusov A A， Atikyan G， Rozelle D M , et al. Force rebalance, whole angle, and self-calibration mechanization of silicon MEMS quad mass gyro[C]// 2014 International Symposium on Inertial Sensors and Systems (ISISS). IEEE, 2014.

[7] Trusov A A， Atikyan G， Rozelle D M , et al. Flat is not dead: Current and future performance of Si-MEMS Quad Mass Gyro (QMG) system[C]// 2014 IEEE/ION Position, Location and Navigation Symposium - PLANS 2014. IEEE, 2014.

[8] Taheri-Tehrani P , Kline M , Izyumin I , et al. Epitaxially-encapsulated quad mass gyroscope with nonlinearity compensation[C]// 2016 IEEE 29th International Conference

on Micro Electro Mechanical Systems (MEMS).IEEE, 2016:966-969.

[9] 夏敦柱，孔伦,虞成.四模态匹配三轴硅微陀螺仪[J].光学精密工程，2013,21(9): 2326-2332.

[10] Wisher S， Shao P， Norouzpour-Shirazi A , et al. A high-frequency epitaxially encapsulated single-drive quad-mass tri-axial resonant tuning fork gyroscope[C]// 2016 IEEE 29th International Conference on Micro Electro Mechanical Systems (MEMS). IEEE, 2016.

[11] Tian Z， Bin Z， Peng Y , et al. Optimal Design of a Center Support Quadruple Mass Gyroscope (CSQMG)[J]. Sensors, 2016, 16(5):613.

[12] 王永，孟冰，陈旭辉,et al.一种环式分布的四质量块微机械陀螺研究[C]W12018 惯性技术发展动态发展方向研讨会文集.2018:174-177.

[13] Wu G， Chua G L， Singh N , et al. A Quadruple Mass Vibrating MEMS Gyroscope With Symmetric Design[J]. IEEE Sensors Letters, 2018, 2:1-4.

[14] 胡恒之. 双解耦微机械陀螺设计,仿真及优化[D]. 浙江大学.

[15] 朱辉杰. 线性调谐微机械陀螺驱动和检测技术的研究[D]. 浙江大学.

二、开题报告

1 问题提出的背景

1.1 背景介绍

陀螺仪的概念是由莱昂.傅科于1850年首次提出的，他在研究中发现处于高速转动中的转子其旋转轴的方向不会发生变化，利用这一特性，陀螺仪先后被应用于航海、航空乃至军事导弹领域的惯性制导。而随着科技的不断发展，微电子技术的出现使得器件越来越小型化，在此基础上，基于科里奥利效应的微陀螺仪逐渐兴起。微陀螺仪与传统陀螺仪的导航原理不同，传统陀螺仪是直接利用旋转轴指向的稳定性，而微陀螺仪是通过科氏效应来获取外界输入到载体的角度从而实现定位。随着陀螺仪相关理论的不断完善以及技术的革新，微陀螺仪的结构缺陷问题逐渐得到很好的解决，其各项指标也越来越接近惯导级，同时，在不断深入的研究下，也衍生出众多的类型。

自微陀螺仪首次应用以来，逐渐成为各大领域不可或缺的重要器件。在惯性导航领域，微陀螺仪可以提供准确的位置信息，确保航海、航空以及航天的顺利运行，同时，还可以搭载在军事导弹上实现精准的轨道控制；在消费电子领域，作为稳定器，微陀螺仪可以实现图像拍照的防抖，增强照片的清晰度，也可以通过重力感应实现各类飞行、竞技游戏的位移操作，提升游戏体验效果。可以看到微陀螺仪在各个领域的广泛应用使我们的出行和工作越来越便利。

MEMS 陀螺仪大多采用基于科氏效应的线性或扭转振动结构来检测外角速率。MEMS 陀螺仪的机械振动会造成短期的输出误差，降低设备的性能。因此，对环境噪声(振动、加速度和冲击)的高抑制是 MEMS 陀螺仪可靠运行的必要条件。为了解决这些问题，四质量块 MEMS 陀螺被提出，相对于一般的单质量块陀螺和音叉陀螺，四质量块陀螺不仅解决了单质量块陀螺存在的的共模干扰问题，且由于四质量块结构的完全对称性，双质量块因驱动、检测模态的不对称所导致的两种模态固有频率差异以及检测模态振

幅较小问题也得到了解决，并显著降低了振动和加速度误差。随着科技的发展，各种传感器的精度要求越来越高，环境适宜性要求亦越来越高，四质量块微陀螺仪在这一领域的独特优势决定了其之后发展的必要性与必然性。

1.2 本研究的目的和意义

从结构和工艺上来看，传统单质量块虽然结构简单，易于加工，但是存在很大的共模干扰，陀螺仪的整体性能上限较低;在此基础之上，双质量块结构由于可以进行差分检测，能有效地消除环境等产生的共模信号，但是由于双质量块结构在驱动、检测模态上的不对称性，其两种工作模态的固有频率有一定的差异，频率分裂大，导致检测模态的振幅相对较小。而本项目设计的四质量块结构将兼顾双质量块微陀螺的优点，在保持高环境鲁棒性的同时也使得结构有较高的对称性，加工工艺也比较成熟，易于批量化生产。

本论文以微机械陀螺的四质量块结构为研究对象，通过理论分析，仿真计算等手段，从机械结构层面对微机械陀螺的动力学等效模型进行研究，致力于设计出锚区受力平衡，锚区损耗较小，具有较大的品质因子，在受到冲击扰动时，能消除冲击扰动影响的基于 SOG 的结构解耦四质量块陀螺，从而实现高精确度、低能量耗散和高共模加速度抑制的成果。

2 论文的主要内容和技术路线

2.1 主要研究内容

本文主要针对MEMS 陀螺仪，提出了一种基于SOG的结构解耦四质量块微陀螺仪的结构设计以及仿真改进，研究内容如下所述。

1) 四质量块结构主要有质量块、支撑锚点、驱动和检测框架、梳齿电极、同步耦合杠杆以及弹性梁六个部分。四质量块涉及的结构参数较多，有些结构对整个器件的性能影响不大，例如驱动和检测框架等;有些结构参数可以根据经验选取，例如器件厚度，锚点高度，电容间隙等;还有一些是设计整个器件的关键参数，必须通过仿真分析并不断优化才能确定，比如弹性梁等。因此，本组重点进行四质量块微陀螺仪的具体结构设计，从耦合杠杆、

解耦梁、连接梁这三个主要结构部件进行结构和参数的确定，对其进行较为详细的刚度分析。

a) 连接梁的设计

研究连接梁的设计方法,包括连接梁几何参数与其等效刚度之间的关系，以及对模态的影响。目前，MEMS 硅微工艺下的弹性梁主要有直梁、L 形梁、U 形梁以及折叠梁等几种类型，通过对这四类连接梁的对比分析，设计优化，实现相邻质量的反相运动。

b) 杠杆的设计

四质量块的实质其实就是双音叉结构,同步耦合杠杆的作用主要是将其连接。理想情况下四质量块的两个音叉应该是互不干扰的，但是实际上,由于加工误差和电路噪声等都会导致两个音叉结构在驱动模态或检测模态下的运动上有细微的差别，通过杠杆机构将其耦合，从而保证两个音叉结构的同步性,可以有效地抑制四质量块微陀螺仪的两个工作模态在运动上的不一致性,从而进一步地减小四质量块微陀螺仪的频率分裂。

研究同步耦合杠杆的设计，主要包括杠杆与锚点的连接方式等。通过对连接处使用不同梁的组合设计，并多次实验优化，以达到最优的铰链效果。

c) 解耦梁的设计

研究解耦梁的设计方法,包括解耦梁的主要几何参数与其等效刚度之间的关系，以及对于中心质量旋转性的抑制作用，通过对于解耦梁的设计优化，抑制中心质量旋转，解除质量块和驱动框架检测框架之间自由度的耦合。

2) 驱动与检测之间的模态耦合对陀螺仪的零偏有很大的影响，一般来说，解耦可以从结构和电路两方面来实现，但是电路解耦的方式对控制电路的要求很高，而且所能达到的解耦程度有限，目前主要是从结构上来降低驱动模态和检测模态之间的耦合效应。在完成上述三个主要连接结构初步设计后，为了达到较为理想的解耦效果，对其结构和刚度配比进行仿真分析，进一步优化参数，已达到更好的结构解耦效果。

3) 按照之前设计的结构对于四质量块进行整体的仿真模拟，确定四质量块陀螺两个模态及其固有频率，测量驱动模态与检测模态的Q值。并和单质量块陀螺、音叉陀螺相比较，研究四质量块陀螺中对阻尼的改善，对锚区的影响，抗冲击特性，分析影响产生的原因与进一步加强四质量陀螺优势的方法。

2.2 技术路线

1、连接梁的设计

连接梁的作用是连接相邻质量块并保证实现相邻质量的反相运动。为了完成对连接梁的设计，首先进行文献调研，然后根据材料力学理论推导其等效刚度计算公式。

2、杠杆的设计

杠杆的作用是保证两个音叉结构同步性并抑制四质量块微陀螺仪的两个工作模态在运动上的不一致性，从而进一步减小陀螺仪的频率分裂。为了完成对杠杆的设计，首先进行文献调研，整理不同耦合杠杆的设计方式，然后在此基础上根据材料力学理论推导其等效刚度计算公式。

3、解耦梁的设计

解耦梁的作用是抑制中心质量的旋转，为了完成对连接梁的设计，首先进行文献调研，整理不同解耦梁的设计方式，然后根据材料力学理论推导其等效刚度计算公式。

4、主要结构仿真与参数优化

等效刚度公式建立完成后，对完整四质量块，在COMSOL中验证连接梁、杠杆和解耦梁对模态的影响以及三者的等效刚度。结合理论公式，优化连接梁的参数，以获得理想工作模态。

5、四质量块微陀螺仪整体结构的仿真分析

按照之前设计的结构对于四质量块进行整体的仿真模拟，在COMSOL中搭建微机械陀螺模态仿真平台，进行模态仿真、重力过载仿真、热弹性阻尼Q值仿真以及谐响应分析，以确定四质量块陀螺两个模态及其固有频率，研究在不同重力过载下的抗冲击性能，计算驱动模态与检测模态的Q值。

将四质量块陀螺与单质量块陀螺、音叉陀螺相比较，研究四质量块陀螺中对阻尼的改善，对锚区的影响，抗冲击特性的提升，分析影响产生的原因与进一步加强四质量陀螺优势的方法。

2.3 可行性分析

1) 微机械陀螺仪的研究已经持续了几十年，虽然四质量块陀螺属于较为较为新颖的类型，但其结构与单质量块与双质量块陀螺有较大的相似之处，可以在其基础上展开研究。国内外对于四质量块陀螺的研究资料也较为丰富。
2) 如今随着科技的发展，陀螺仪的制作工艺日新月异，各种仿真软件（如COMSOL与ANSYS等）具有非常出色的多物理场耦合仿真功能，其出现为陀螺仪结构模拟实验提供了良好的平台。
3) 浙江大学微小卫星研究所在MEMS四质量块陀螺的研究方面已经有比较成熟的成果，本文主要目标是研究如何在其基础上进行优化。

综上所述，本项目研究可行性具有充足的保障。

3 研究计划进度安排及预期目标

3.1 进度安排

现计划项目于开题答辩后开展具体工作。将在寒假期间进行MEMS四质量块陀螺结构、耦合特性以及解耦方式相关知识的学习。

春学期第一、二周完成解耦梁设计、杠杆设计以及连接梁设计，春学期第三、四周利用 COMSOL 完成主要结构的仿真以及参数优化，结合理论公式，优化连接梁的参数，以获得理想工作模态。第五、六周对于四质量块进行整体的仿真模拟，在 COMSOL 中搭建微机械陀螺模态仿真平台，进行模态仿真、重力过载仿真、热弹性阻尼 Q 值仿真以及谐响应分析。之后对以上所有实验进行整理、总结以及毕业论文的撰写。

3.2 预期目标

本文以微机械陀螺的四质量块结构为研究对象，通过理论分析，仿真计算等手段，从机械结构层面对微机械陀螺的动力学等效模型进行研究，以解决单质量块陀螺存在的的共模干扰问题，且由于四质量块结构的完全对称性，双质量块因驱动、检测模态的不对称所导致的两种模态固有频率差异以及检测模态振幅较小问题也将得到解决。本文致力于设计出锚区受力平衡,锚区损耗较小，

具有较大的品质因子,能消除冲击扰动影响的基于 SOG 的结构解耦四质量块陀螺。

4 参考文献

[1] Jia, Xukai, Ding, et al. Automatic Frequency Tuning Technology for Dual-Mass MEMS Gyroscope Based on a Quadrature Modulation Signal.[J]. Micromachines, 2018.

[2] Trusov A A , Member, IEEE, et al. Low-Dissipation Silicon Tuning Fork Gyroscopes for Rate and Whole Angle Measurements[J]. IEEE Sensors Journal, 2011, 11(11):2763-2770.

[3] Trusov A A , Atikyan G , Rozelle D M , et al.Flat is not dead: Current and futureperformance of Si-MEMS Quad Mass Gyro (QMG) system[C] 2014 IEEE/IONPosition, Location and Navigation Symposium - PLANS 2014.IEEE,2014:252-258.

[4] Trusov A A ,Atikyan G , Rozelle D M , et al.Force rebalance,whole angle,andself-calibration mechanization of silicon MEMSquad mass gyro[C]!I 2014International Symposium on Inertial Sensors and Systems (ISISS).IEEE,2014.

[5] Trusov A A， Atikyan G， Rozelle D M , et al. Force rebalance, whole angle, and self-calibration mechanization of silicon MEMS quad mass gyro[C]// 2014 International Symposium on Inertial Sensors and Systems (ISISS). IEEE, 2014.

[6] Trusov A A， Atikyan G， Rozelle D M , et al. Force rebalance, whole angle, and self-calibration mechanization of silicon MEMS quad mass gyro[C]// 2014 International Symposium on Inertial Sensors and Systems (ISISS). IEEE, 2014.

[7] Trusov A A， Atikyan G， Rozelle D M , et al. Flat is not dead: Current and future performance of Si-MEMS Quad Mass Gyro (QMG) system[C]// 2014 IEEE/ION Position, Location and Navigation Symposium - PLANS 2014. IEEE, 2014.

[8] Taheri-Tehrani P , Kline M , Izyumin I , et al. Epitaxially-encapsulated quad mass gyroscope with nonlinearity compensation[C]// 2016 IEEE 29th International Conference on Micro Electro Mechanical Systems (MEMS).IEEE, 2016:966-969.

[9] 夏敦柱，孔伦,虞成.四模态匹配三轴硅微陀螺仪[J].光学精密工程，2013,21(9): 2326-2332.

[10] Wisher S， Shao P， Norouzpour-Shirazi A , et al. A high-frequency epitaxially encapsulated single-drive quad-mass tri-axial resonant tuning fork gyroscope[C]// 2016 IEEE 29th International Conference on Micro Electro Mechanical Systems (MEMS). IEEE, 2016.

[11] Tian Z， Bin Z， Peng Y , et al. Optimal Design of a Center Support Quadruple Mass Gyroscope (CSQMG)[J]. Sensors, 2016, 16(5):613.

[12] 王永，孟冰，陈旭辉,et al.一种环式分布的四质量块微机械陀螺研究[C]W12018 惯性技术发展动态发展方向研讨会文集.2018:174-177.

[13] Wu G， Chua G L， Singh N , et al. A Quadruple Mass Vibrating MEMS Gyroscope With Symmetric Design[J]. IEEE Sensors Letters, 2018, 2:1-4.

[14] 胡恒之. 双解耦微机械陀螺设计,仿真及优化[D]. 浙江大学.

[15] 朱辉杰. 线性调谐微机械陀螺驱动和检测技术的研究[D]. 浙江大学.

[16] 李敏阳, 张卫平, 谷留涛,等. 结构解耦四质量块微陀螺仪的设计与制备[J]. 半导体光

电, 2020, 41(2):5.

三、外文翻译

对称设计的四质量振动 MEMS 陀螺仪

作者：吴国强、耿丽娟、纳瓦布·辛格、顾元东

新加坡 Innovis 科学、技术和研究机构微电子研究所，138634

摘要：本文介绍了一种新型的对称设计的微机电系统（MEMS）四重质量陀螺仪（QMG）。与酒杯振动陀螺仪类似，所报道的 QMG 在驱动和传感模式下均具有对称结构设计。使用中心耦合弹簧和四个锥形杆将四重质量耦合在一起，以同步反相驱动运动。所报告的 QMG 通过机械抑制大大降低了加速度和振动引起的共模信号。驱动和传感方向上的动量和扭矩平衡有助于通过锚实现超低能量耗散，从而实现高质量因数（Q）和高分辨率。实验测量结果表明，QMG 表现出 5.9°/h 的艾伦方差偏差不稳定性和约 0.28°/√h 的白噪声水平，分别由来自集成电路的闪烁和热噪声控制。测量的比例因子为 94.98 LSB/(°/s) 在±300°/s 的满标度范围内，非线性小于 600 ppm。本文报告的 QMG 展示了一种实现高精度惯性测量装置的潜在高性能陀螺仪设计的新方法。

关键词：机械传感器，MEMS 陀螺仪，科罗伊效应，四重惯性质量，振动不敏感，对称设计。

一、 导言

近年来，微机电系统(MEMS)陀螺仪以其体积小、性能好、批量生产能力强等优点受到人们的广泛关注。MEMS 陀螺仪已经主导了广泛的消费市场，如手机、平板电脑、玩具、游戏和体育运动。然而，为了进入高端汽车和工业应用，需要更高的性能，如汽车的防滚转和电子稳定控制系统、海上导航、稳定系统和工业钻井。

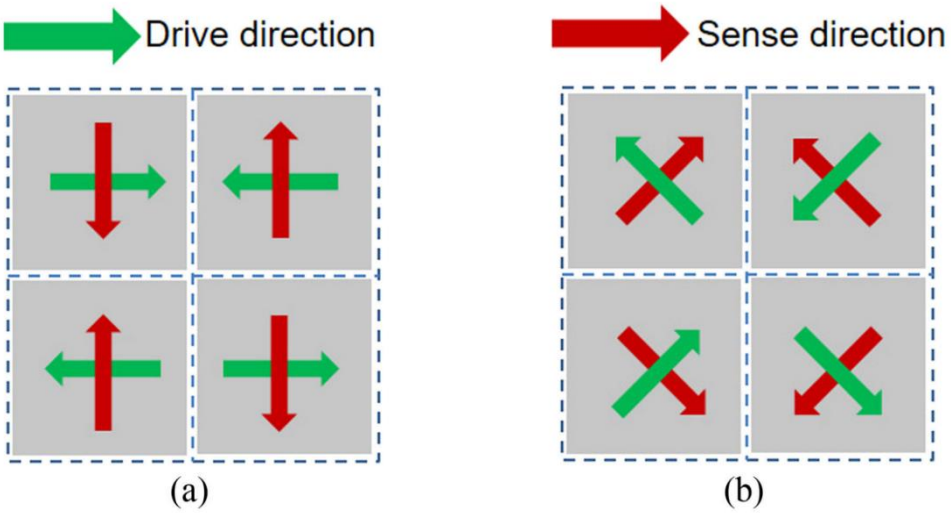

图 1 两种 QMG 设计的示意图。 (a) 当前的 QMG 设计：一列中的两个惯性质量彼此靠近，而另一列中的另外两个惯性质量彼此远离。 (b) 提议的 QMG 设计：一个对角线方向的两个惯性质量相互远离，而另一个对角线方向的另外两个惯性质量相互靠近。

MEMS 陀螺仪大多采用基于科氏效应的线性或扭转振动结构来检测外角速率。振动 MEMS 陀螺仪最大的误差来源之一是振动灵敏度[6]。陀螺仪的机械振动会造成短期的输出误差，降低设备的性能。因此，对环境噪声(振动、加速度和冲击)的高抑制是 MEMS 陀螺仪可靠运行的必要条件。采用两反相振动惯性质量的差动传感器设计，可以显著降低振动和加速度误差。然而，采用差分双质量设计[7]不能消除由角加速度引起的故障信号。为了进一步提高 MEMS 的抗振能力,Analog Devices Inc.[7]提出了一种基于双差分设计的四核 MEMS 陀螺仪。由 Shkel et al.[8]-[10]开发的具有四个对称解耦齿的四质量陀螺仪(QMG)具有超低的能量耗散和高的共模加速度抑制，如图 1(A)所示。报道了一种中心支撑的四重质量陀螺仪，并预测该陀螺仪将取得良好的性能。体声波陀螺仪由于其固有的高刚度和鲁棒性[5]，在环境刺激下也表现出了高性能。萨基姆已经开发了一种新型振动陀螺仪(Quapason)使用四束金属谐振器。它具有三维轴对称，对外界机械振动的灵敏度很低。

在本文中,我们报道了一种新型的全对称设计的MEMS QMG,如图1(b)所示。它利用了酒杯陀螺仪的理想对称设计和音叉陀螺仪的大惯性质量。与[12]中相同的工作模式形状，这里演示的 QMG 在驱动和传感方向上都具有理想的对称设计。驱动和传感方向的动量和扭矩平衡有助于通过锚的超低能量耗散，并导致对外部振动和冲击的高排斥性。

二、 设计和操作原理

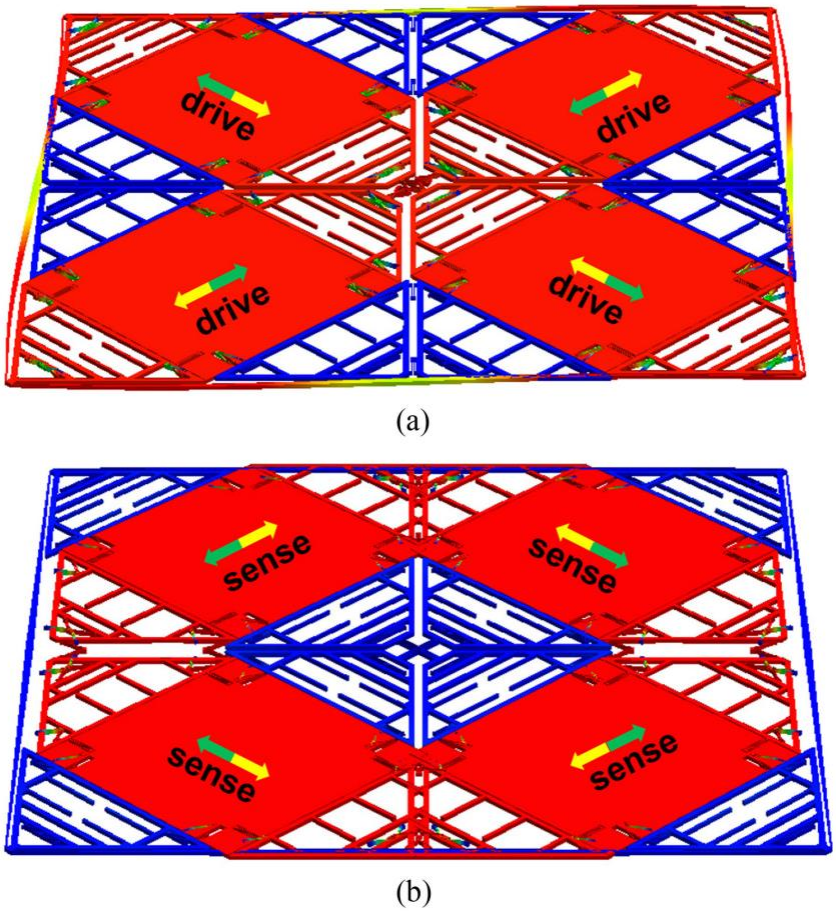

图 2 QMG 的模拟振型变形。 (a) 驾驶模式。 (b) 传感模式。 对称、反相驱动和传感模式导致完全的动态平衡、低能量耗散、良好的抗冲击和振动抑制能力。 红色区域表示振动模式中发生的最大位移。

图 2 说明了使用 CoventorWare 通过有限元方法获得的报告 QMG 的模拟模式形状变形。与酒杯陀螺仪类似，所报道的 QMG 在驱动和传感模式下均采用对称设计。在提议的设计中，QMG 由一个外框架和四个惯性质量组成，作为一个阵列，包括外框架内的两行两列。在驱动模式下，一个对角线方向的两个惯性质量体相互远离，而另一个对角线方向的另外两个惯性质量体相互靠近，如图 2（a）所示。四重惯性质量使用中央耦合弹簧和四个锥形杠杆耦合在一起，以同步反相驱动运动。在感测模式下，第一对角线方向的两个惯性质量块在垂直于第一对角线的方向上相互远离。第二对角线方向的另外两个惯性质量在垂直于第二对角线的方向上相互远离运动，如图 2（b）所示。驱动模式采用梳齿，传

感模式采用平行板。在本文中，采用模式拆分方法以实现较大的所需带宽。驱动模式和传感模式的模拟谐振频率分别为 13961 Hz 和 15054 Hz。最近的非期望平面外模式的模拟谐振频率为 19094 Hz。

这种结构实现了理想的对称设计。报道的 QMG 设计减少了传感器不对称的影响，并且对外部振动和冲击有很大的抑制作用。此外，驱动和传感方向上的动量和扭矩平衡有助于通过锚实现超低能量耗散,从而实现高品质因数(Q)和高分辨率。

三、 制造和测量

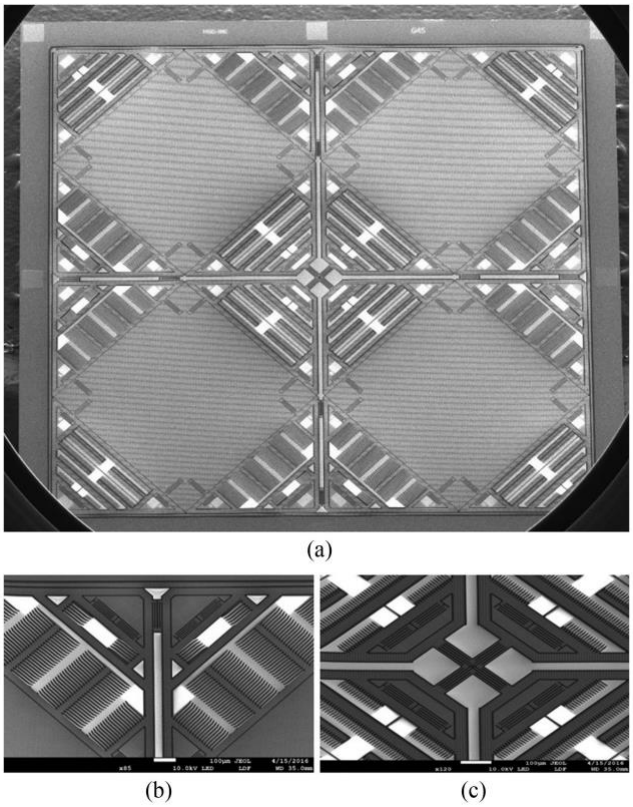

图 3 所制备的 QMG 的 SEM 图像。（a）总体结构。四个惯性质量与外框和耦合弹簧耦合在一起。（b）感应电极和锥形杆的特写视图。（c）驱动电极和中央耦合弹簧的特写图。

QMG 是基于具有 30 微米厚器件层的 8 英寸绝缘体上硅晶片使用两个掩模工艺制造的。第一个掩模定义了焊盘，第二个掩模形成了 MEMS 结构，然后是深反应离子蚀刻 (DRIE)。最后，使用蒸气氟化氢干蚀刻释放可移动结构。图 3 显示了制造的 QMG 的扫描电子显微镜 (SEM) 图像。图 3 清楚地显示了四个惯性质量和耦合弹簧。测量的换能间隙宽度为 1.2 um。测量的感应、驱动和监测电极的平均电容分别为 6.2 pF、2.9 pF 和 2.8 pF。 QMG 的尺寸为 5.8 mm

x 5.8 mm x 0.7 mm（宽 x 长 x 厚）。

切割后，QMG 芯片被真空封装在陶瓷封装中，以减少空气阻尼[13]。封装载体内的压力小于 0.01 mbar [14]。QMG 的频率响应是用动态信号分析仪测量的。测量的驱动模式和制造 QMG 的传感模式的谐振频率为 12 940 Hz 和 13 分别为 384Hz。由于 DRIE 过程中的临界尺寸损失，测量频率小于模拟值（驱动模式和传感模式分别为 13 961 Hz 和 15 054 Hz）。驱动模式下的测量值为 90 300，感测模式下为 39 200。驱动模式中使用的梳状指显示出更大的 Q 值，因为主要的空气阻尼机制是滑动阻尼，而不是挤压阻尼。

四、 陀螺系统测量

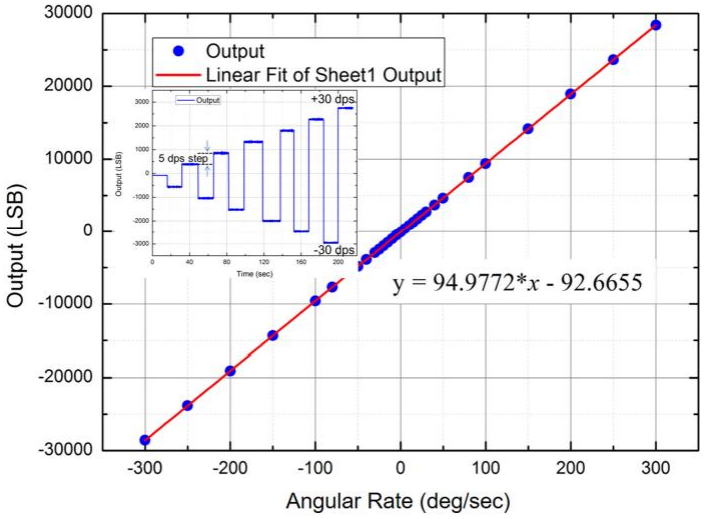

图 4 QMG 的测量角速率响应。比例因子的测量值为 94.98 LSB/(°/s)，且在±300°/s 的满标度范围内，标度因数非线性小于 600 ppm。

封装的 QMG 安装在印刷电路板上以与集成电路（IC）连接。报道的 QMG 在模式分离方法中运行，其中感测谐振频率略大于驱动谐振频率以实现所需的带宽 [15]。本文使用的读出 IC 购自 TUMEMS technologies。它具有激励和传感电子设备，以获得 MEMS 陀螺仪的角速率特性。激励回路使用数字锁相回路，以锁定在驱动谐振频率中振动的可移动驱动框架和科里奥利框架。可移动结构通过使用自动增益控制电路保持恒定的驱动幅度。传感电子通过电容到电压级的差分低噪声电荷放大器从传感电极的输出中提取转速。同步解调后，采用高分辨率 16 位模数转换器将输出信号数字化，并将检测到的角速率输出到 I2C 接口。可编程带通滤波器也包含在驱动回路和感测回路中，以提高信噪比。

速率表用于将角速率应用于 QMG 以获得其角速率响应。图 4 示出了 QMG 的测量角速率响应。输入角速率从-300°/s 到+300°/s。电路的数字输出用 I2C 接口记录。测量的比例因子为 94.98LSB/(°/s)。在±300°/s 的满量程范围内，比例因子非线性小于 600 ppm，QMG 系统对角速率旋转的正负输入阶跃的测量响应如图 4 的插图所示。

为了评估 MEMS 陀螺仪系统的偏置不稳定性和角度随机游走（ARW），在室温下收集了 1.2 小时的零率输出（ZRO）数据。陀螺仪系统的根艾伦方差曲线如图 5 所示。插图是从 QMG 系统收集的 ZRO 的时间片。根艾伦效价曲线表明 QMG 在平均约 10 秒的时间内显示出 5.9°/h 的偏置不稳定性。QMG 的 ARW 测量为 0.28°/√h，受电噪声白噪声的限制。

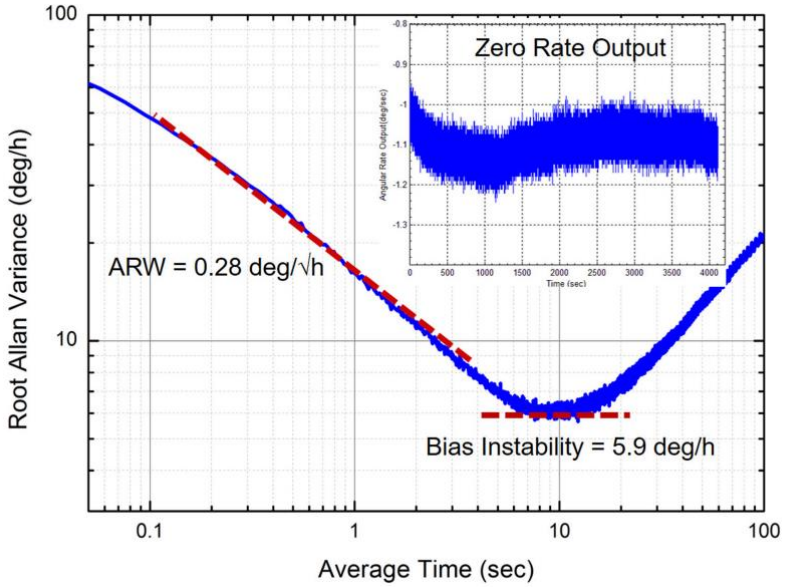

图 5 QMG **系统的根艾伦方差图。 获得了** 5.9°/h **的偏置不稳定性和** 0.28°√h **的** ARW。

通过测试其对外部冲击的反应，验证了带有 IC 的 QMG 的稳健性。 陀螺仪系统固定在振动台上。振动台沿QMG系统的z轴施加半正弦冲击加速度信号。总共三个半正弦形状的激励信号，幅度为 16 g，持续时间为 11 毫秒，间隔为 10 秒。 图 6 显示了 QMG 系统实测的冲击响应。QMG 系统的最大偏置偏移(峰峰值)约为 4.5°/s,可能是由于制造缺陷的不对称性造成的。表 1 说明了 QMG 系统的实测参数。

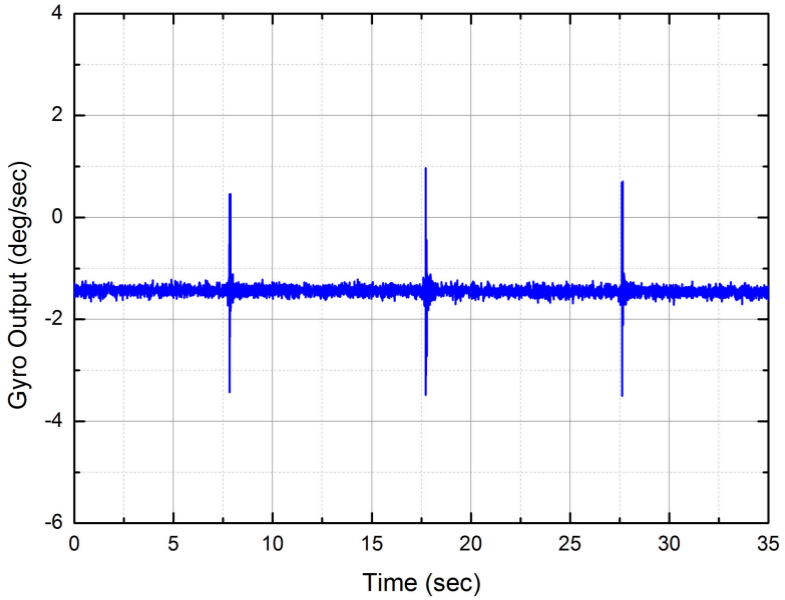

图 6 在幅度为 16 g 和持续时间为 11 ms 的三个半正弦冲击加速度信号下测得 QMG 系统的最大偏置偏移

Parameters	Values	Units
Full scale range	±300	deg/sec
Scale factor	94.98	LSB/(deg/sec)
Scale factor non-linearity	600	ppm
Angle random walk	0.28	deg/√h
Bias instability	5.9	deg/h
Maximum bias shift under shock (amplitude: 16 g; duration: 11 ms)	4.5	deg/sec

表 1 QMG 系统的测量参数。

五、 结论

我们在本文中报道了一种在驱动模式和传感模式下均具有理想对称设计的 MEMS QMG。四重质量块使用中央耦合弹簧和四个锥形杠杆耦合在一起，以同步反相驱动运动。 QMG 对外部振动和冲击不敏感。 报道的设计为硅基振动 MEMS 陀螺仪进入高端惯性导航应用铺平了道路。

参考文献

[1] K.Liu et al., “The devel-opment of micro-gyroscope technology,” J. Micromech. Microeng., vol. 19, no. 11, Oct. 2009, Art. no. 113001.

[2] F. Ayazi and K. Najafi, “A HARPSS polysilicon vibrating ring gyroscope,” J. Microelectromech. Syst. vol. 10, no. 2, pp. 169–179, Jun. 2001.

[3] S. E. Alper, Y. Temiz, and T. Akin, “A compact angular rate sensor system using a fully decoupled silicon-on-glass MEMS gyroscope,” J. Microelectromech. Syst., vol. 17, no. 6, pp. 1418–1429, Dec. 2008.

[4] S.Sonmezoglu et al.,“Single-structure micromachined 3-axis gyroscope with reduced drive-force coupling,” IEEE Electron Device Lett., vol. 36, no. 9, pp. 953– 956, Sep. 2015.

[5] D. E. Serrano et al., “Substrate-decoupled, bulk-acoustic wave gyroscopes: Design and evaluation of next-generation environmentally robust devices,” Microsyst. Nanoeng., vol. 2, Feb. 2016, Art. no. 16015.

[6] H. Weinberg, “Gyro mechanical performance: The most important parameter,” Tech. Art., Analog Devices, Norwood, MA, USA, Sep. 2011. [Online]. Aviliable: http://www.analog.com/media/en/technical-documentation/tech-articles/MS-2158. pdf

[7] M. Fuldner, “Vibration-immune multi-core MEMS gyroscopes are improving auto ¨ safety,” Analog Devices, Norwood, MA, USA.

[8] A. Trusov, I. Prikhodko, S. Zotov, and A. Shkel, “Low-dissipation silicon tuning fork gyroscopes for rate and whole angle measurements,” IEEE Sens. J., vol. 11, no. 11, pp. 2763–2770, Nov. 2011.

[9] A. A. Trusov et al., “Flat is not dead: Current and future performance of Si-MEMS quad mass gyro (QMG) system,” in Proc. IEEE/ION Position Location Navigat. Symp., May 2014, pp. 252–258.

[10] S. A. Zotov, A. A. Trusov, and A.M. Shkel, “High-range angular rate sensor based on mechanical frequency modulation,” J. Microelectromech. Syst., vol. 21, no. 2, pp. 398–405, Apr. 2012.

[11] B. Zhou, T. Zhang, P. Yin, Z. Y. Chen, M. L. Song, and R. Zhang, “Innovation of flat gyro: Center support quadruple mass gyroscope,” in Proc. IEEE Int. Symp. Inertial Sens. Syst., Laguna Beach, CA, USA, Feb. 22–25, 2016, pp. 1–4.

[12] P. Leger, “QuapasonT M—A new low-cost vibrating gyroscope,” in Proc. 3rd St. Petersburg Int. Conf. Integr. Navigat. Syst., Saint Petersburg, Russia, May 1996, p. 15.

[13] M. H. Asadian, S. Askari, and A. M. Shkel, “An ultra-high vacuum packaging process demonstrating over 2 million Q-factor in MEMS vibratory gyroscopes,” IEEE Sens. Lett., vol. 1, no. 6, Dec. 2017, Art. no. 6500104.

[14] G. Q. Wu, D. H. Xu, B. Xiong, L. F. Che, and Y. L. Wang, “Design, fabrication and characterization of a resonant magnetic field sensor based on mechanically coupled dual-microresonator,” Sens. Actuators A: Phys., vol. 248, pp. 1–5, Sep. 2016. 、

[15] G. Q. Wu, G. L. Chua, and Y. D. Gu, “A dual-mass fully decoupled MEMS gyroscope with wide bandwidth and high linearity,” Sens. Actuators A: Phys., vol. 259, pp. 50– 56, Mar. 2017

一种高频外延封装单线质量三轴谐振音叉陀螺仪

作者:S.Wisher,P.Shao,A,A.Norouzpour-Shirazi,Y.Yang, E.Ng,I.Flader2,Y.Chen2,D.Heinz2,T.Kenny2,and F.Ayazi

Georgia Institute of Technology, Atlanta, GA, USA

Stanford University,Palo Alto,CA,USA

摘要：本文介绍了一种单驱动工作模式的“高频”谐振三轴音叉陀螺仪。该四质量器件是在一个2x2 mm²真空封装模具上实现的,使用epi-seal工艺，使其成为最小的圆片级封装的三轴陀螺之一。与常规谐振式TFGs相比，谐振频率设计为相对较高(~138 kHz)，允许模式匹配操作的高带宽，并增强了抗冲击和振动。结果表明，对所有三个轴都具有灵敏度，z轴为模式匹配操作，X轴和Y轴为模式分裂。

一、 导言

微机械陀螺仪广泛应用于从汽车安全到相机的图像稳定等许多应用领域，随着MEMS陀螺仪技术的进步，应用范围也在扩大。MEMS陀螺仪设计中最常见的类型是 TFG，这是一种可以在模式匹配或模式分裂条件下操作的梭式证明质量设计。虽然分模操作允许非常宽的可调动态范围和相对良好的跨温度标度因子稳定性，但它的应用受到差信噪比性能的限制。模式匹配操作通过Q放大可以显著提高机械信噪比(SNR),但高Q模式匹配陀螺仪的主要限制是开环机械带宽小导致动态范围减小。通过增加模式匹配谐振陀螺仪的工作频率，可以提高机械带宽[1]-[3]。

多自由度(DOF)惯性测量单元(IMU)可用于提高GPS性能的平台，在某些情况下，可以完全消除对GPS的需求。多种解决方案被提出以实现用于多自由度IMU 的三轴陀螺仪。传统上，三个独立的单轴陀螺仪模具被定向来检测围绕每个轴的旋转。这种技术，在为所有轴提供非常高性能的同时，需要复杂的封装技术来最小化轴的不对称，同时也需要更大更厚的封装来容纳3d排列的设备。另一种常见的解决方案是在一个普通的[4]模具上实现三个陀螺仪,为成本敏感

的小封装应用提供了一种有效的解决方案。其中，利用单驱动机构同时感知 X、Y 和 Z 旋转的设计通常提供最低的功率。意法半导体和博世都开发了基于[5]，[6]这一概念的设备。

然而，这些设计都是在低频，并受模式匹配条件下的操作限制，以及对冲击和振动的敏感性。本文所介绍的装置是第一次尝试将移动质量谐振式 TFG 的模态频率提高到比传统 TFG 高得多的频率，以增加带宽和动态范围，并提高对冲击和线性振动的抵抗能力。此外，陀螺仪操作扩展到三轴单驱动机构。

二、 高频三轴 TFG

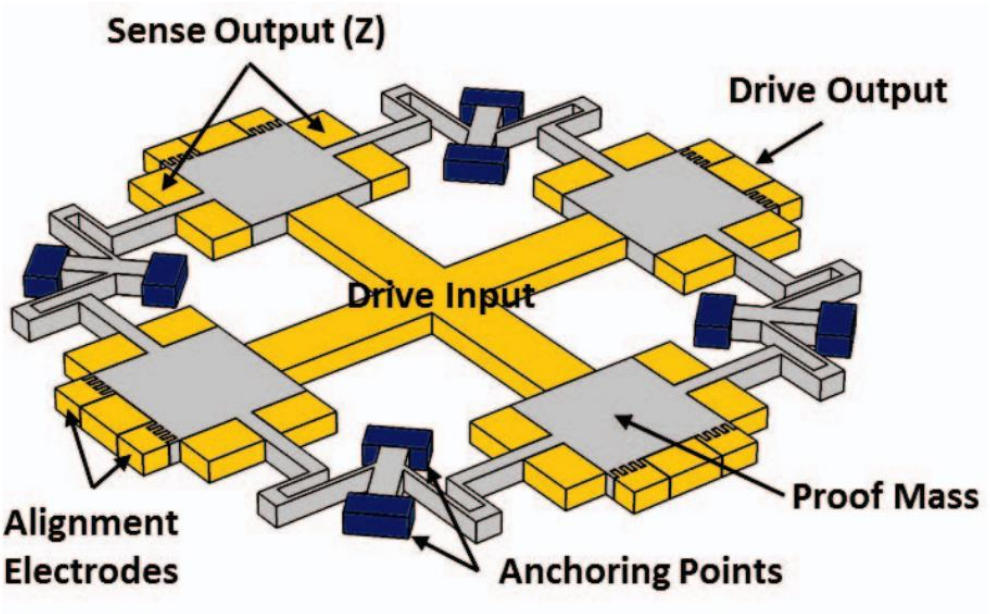

图 1 单驱动四质量三轴 TFG 的示意图，说明电极和锚定点。

与传统的谐振式 TFGs 相比，该器件具有较高的谐振频率(~138kHz)，以提高器件在模匹配条件下的带宽，增强器件对冲击和振动的鲁棒性。对于外部线性振动，设备可以表现出平移运动，在某些情况下，这些外部振动是由频率在 10-20 kHz 范围内的声波干扰引起的，这也是常规谐振式 TFGs 的频率范围。在这样的 TFGs 中，这些平移模的谐振频率通常接近于感觉模和驱动模。当扰动接近于谐振模态频率时，传感输出的不稳定性显著增加。结果表明，将 TFG 谐振频率提高到远高于外部振动频率时，传感输出对外部振动的灵敏度会显著降低。

更高频率器件的另一个好处是，由于更小的弯曲尺寸和证明质量，高频 TFG 设计的尺寸减小；然而，由于侧壁倾斜等工艺缺陷，降低的弯曲尺寸导致共振频

率发生更剧烈的变化。当设计的模式是在彼此的可调谐范围内，这些考虑是特别重要的，因为对应于每个谐振模式的弯曲的尺寸不同。由于侧壁倾斜，可以看到模态共振频率的变化。通过一个具有特征的、可重复的过程，这些频率偏移可以在弯曲的设计中得到补偿。

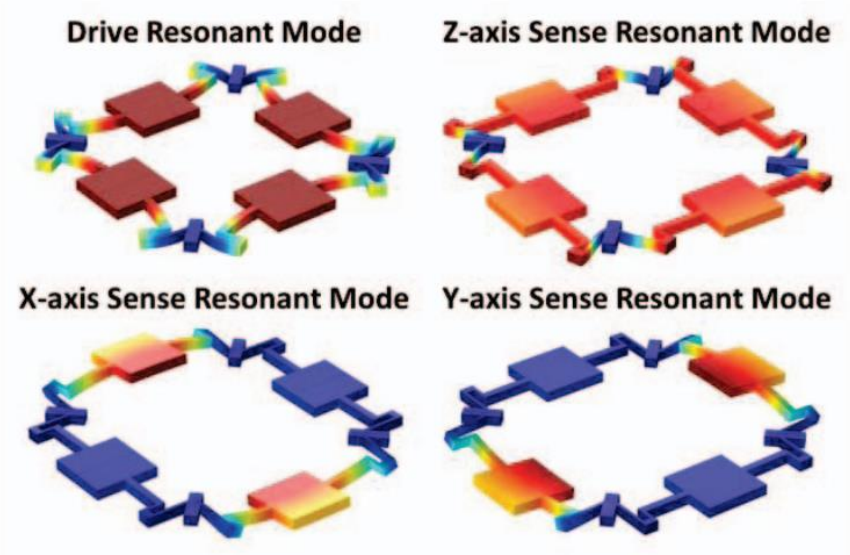

图 2 COMSOL 生成的驱动模式、Z 轴感应模式、X 轴感应模式和 Y 轴感应模式形状图。

虽然大多数 TFG 使用梳状驱动电极进行驱动，但该装置增加的刚度由平行板电极能更有效地驱动,从而更容易施加更大的驱动力并允许灵敏的电流输出。传感模式频率被设计为高于驱动模式，电极设计利用驱动和传感电极的不同电容间隙尺寸来降低 Z 轴传感模式频率，使其比驱动 X 的频率大得多，通过增加极化电压（Vp）使静电弹簧软化，形成 Y 模。这种设计允许 Z 模式与驱动模式相匹配。X 和 Y 模式也可通过增加 Vp 进行调谐，但为了进一步增强静电调谐的灵活性，可向专用顶部电极施加电压，该电极与平面外感测电极相邻。选择了约 138 kHz 的谐振频率，以允许设备足够兼容驱动和感应模式的调谐，同时仍然足够高，以有效抑制振动并增加带宽。还包括对准电极，以减少面内模式的未对准，但为了增加其效果，必须施加更大的力以完全抵消此效果。由于静电力与间隙尺寸之间存在着密切的关系，因此，本工作中的对准电极的有效性需要减小电容间隙尺寸，以提高本设计的稳健性。

三、 制造和包装

该器件是使用斯坦福大学和博世 RTC 研究人员开发的外延密封工艺制造

和晶圆级封装的[7-8]。该工艺从具有 40 um 器件层和 2 umburied 氧化层的 SOI 晶片开始。通过使用深反应离子蚀刻 (DRIE) 在器件层中蚀刻沟槽来定义谐振器轮廓。接下来，沉积牺牲氧化物层以在器件上方形成氧化物间隔层。然后在氧化物层中蚀刻触点，然后沉积第一层硅。形成氮化物插塞以定义顶部电极轮廓。然后在硅帽中蚀刻排气孔，并使用蒸气 HF 释放谐振结构。释放后立即通过沉积最后一层硅将器件密封在外延反应器室中。最后，定义电隔离和金属接触。该过程提供了一个清洁、低压的运行环境，使设备能够实现长期稳定运行[9]。图 3 显示了突出显示工艺层的横截面图，图 4 显示了所提出的 TFG 设计的 SEM。

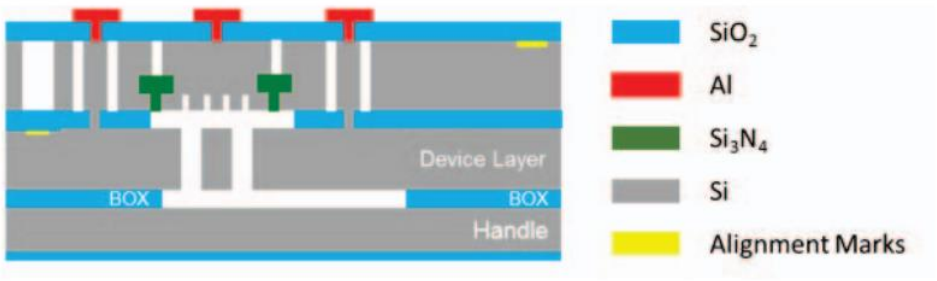

图 3 通过 epi 密封工艺制造的器件各层的横截面图。

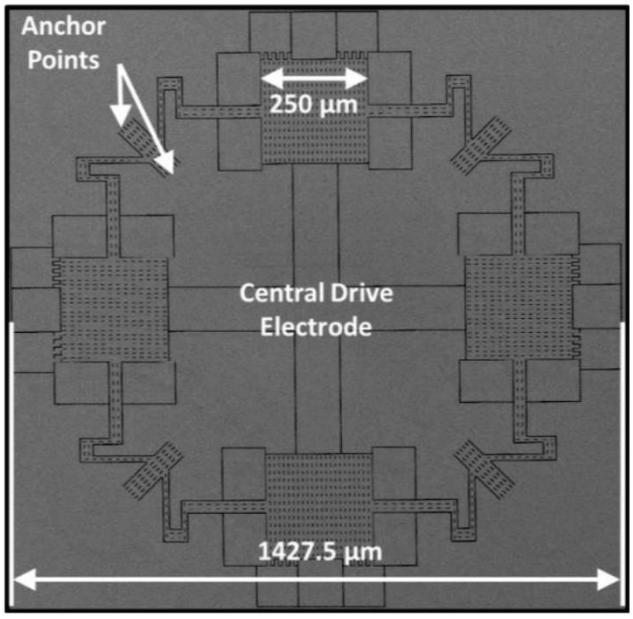

图 4 通过外延密封工艺制造和封装的单驱动三轴 TFG 的顶部 SEM 视图。

四、 实验结果

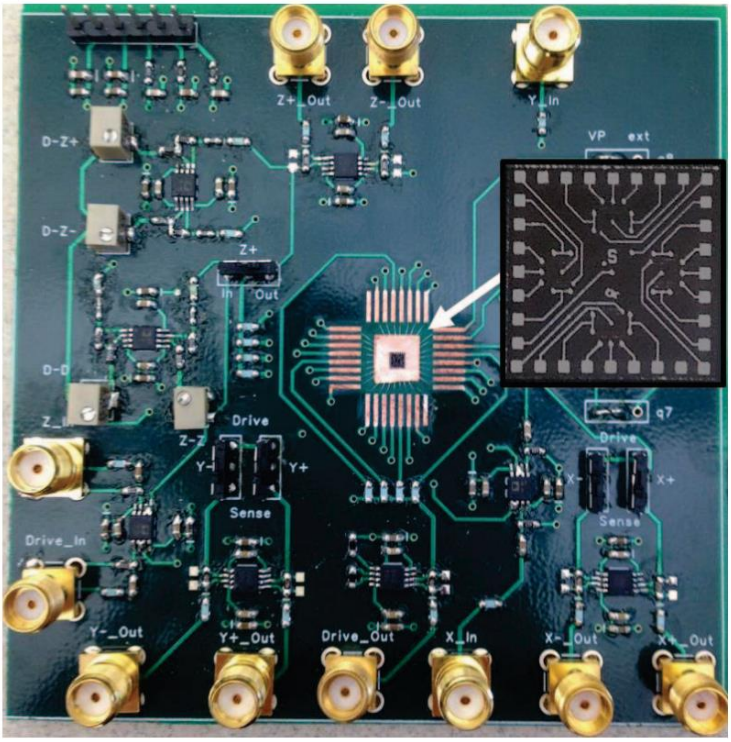

图 5 定制陀螺仪接口 PCB，包括缓冲器、TIA 和馈通消除电路，与锁定放大器和晶圆级封装的三轴 TFG 芯片结合使用。

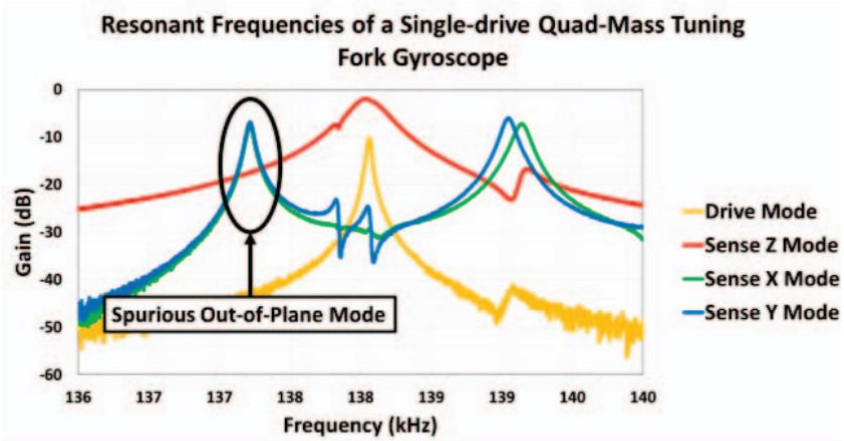

	Drive Mode	Sense Z Mode	Sense X Mode	Sense Y Mode
Frequency (Hz)	138058	138043	139140	139048
Quality Factor	3910	505.0	1181	1360
Bandwidth (Hz)	35.0	273	118	102

图 6 表征数据显示了 Z-检测模式匹配条件下的各种驱动和检测模式峰值，以及 X-和 Y-检测模式分裂。

结果是通过使用 Zurich Instruments HF2LI 锁定放大器获得的，其中 TFG 绑定到如图 5 所示的定制 PCB。每种检测模式的输出电流被提供给跨阻放大器（TIA）以放大速率信号并将其转换为电压。当施加 47.9 V 的 Vp 时，驱动模式和 Z 模式匹配。图 6 显示了调谐后器件的谐振频率，Z 模式频率与驱动模

式的频率静电匹配。 X 和 Y 模式能够通过顶部调谐电极调谐到驱动和感应模式的电平，但是通过分别向 X 和 Y 调谐电极施加 43 V 和 21 V，它们被调谐到频率为大约高 1 kHz，以最大限度地减少面外和面内模式之间的交叉耦合效应。选择这种分频是为了允许驱动模式和 Z 模式落在 X 和 Y 模式之间以及面外杂散模式，以尽可能减少面内和面外模式之间的模式耦合.图 7 显示了输出电流响应旋转的灵敏度曲线。模式匹配 Z 轴灵敏度为 30.5pA/°/s，模式分离 X 轴和 Y 轴灵敏度为 1.40 pA/°/s 和 1.21 pA/°/s。分别。在这种情况下，电容间隙尺寸限制和模式未对准会降低灵敏度。由于模态交叉耦合导致 X 和 Y 模式无法匹配驱动，未来的改进将需要面内和面外模式之间的面外交叉耦合抵消方案以允许匹配 X 和 Y 模式到驱动模式。采用完全模式匹配的三轴 TFG 设计，X 轴和 Y 轴灵敏度可以显着提高。

收集艾伦方差数据来评估每个旋转轴的噪声性能,得到的信息如图 8 所示。角度随机游走（ARW）代表系统的白噪声为旋转，偏置不稳定性代表最佳可实现的偏差漂移。模式匹配的 Z 轴噪声表现类似于 [10] 中提出的 3 轴陀螺仪，其中作者在减少驱动力耦合后，Z 轴的 ARW 达到 0.039°/√s，偏置不稳定性达到 0.042°/s。驱动力耦合和正交耦合都是由于制造缺陷导致模式未对准的结果，它们会导致偏置误差的增加[11]。正交耦合通常远高于速率信号的耦合，如果没有正交去耦的方法，读出电路解调相位的任何小偏移都会导致偏置的明显偏移。因此，为了改进所呈现器件的偏置性能，必须增强正交抵消。

TFG 的高频设计显示 Z 模式的带宽超过 100 Hz。调谐驱动和感应模式的工作频率范围为 138.043 kHz 至 139.140 kHz。增加的操作频率使该陀螺仪具有必要的特性，以抑制经常发生在低得多的频率下的环境声波和超声波干扰。

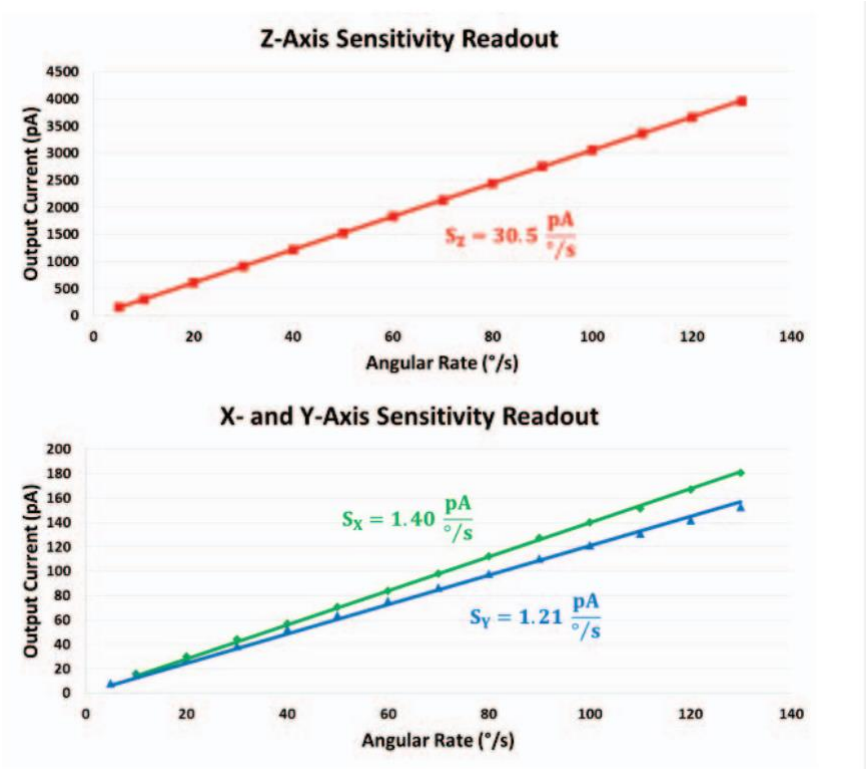

图 7 显示输出电流（pA）与 Z、X 和 Y 轴角速率（/s）关系的灵敏度图。

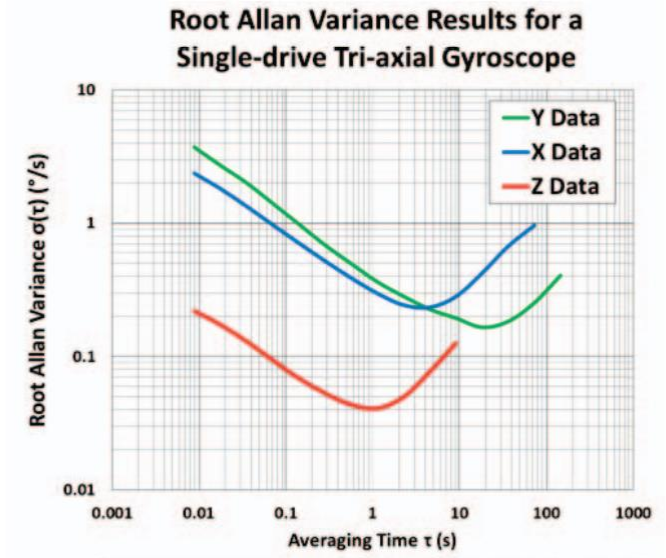

	X-axis	Y-axis	Z-axis
Angle Random Walk (°/√s)	0.292	0.357	0.028
Bias Instability (°/s)	0.226	0.166	0.041

图 8 艾伦方差图，显示了三轴 TFG 每个输出的 ARW 和偏压不稳定性。

五、 结论

这项工作提出了一种在 2x2 mm²晶圆级封装芯片上实现的高频单驱动四质

量 TFG，它显示了所有三个旋转轴的速率灵敏度。在挠曲设计中，工艺引起的模式频移得到了有效补偿，以使谐振频率在模式匹配操作的可调谐范围内。与低频 TFG 相比，高频谐振模式能够更有效地抵抗环境振动，并且能够显著减小器件的尺寸。虽然由于模式分割操作，X 和 Y 感测模式的灵敏度和噪声性能不是最佳的，但该设备仍然能够执行偏压不稳定性的评级标准，并且 Z 感测模式的 ARW 和偏压不稳定性随着模式匹配操作而显示出改善。为了改进这种设计并减少稳定性偏差，必须在今后的工作中制定一种方案来减少模式失调的影响。由于该装置的大刚度，正交消除将需要较小的电容间隙（与 700 nm 相比约 200 nm），以便能够向结构施加较大的力并确保高成品率。

由于该设备的带宽允许非常大的满标度范围，因此可以在不牺牲大带宽优势的情况下提高 Q 值。未来的设备还将具有设计用于更高 Qs 的挠曲，以确保设备仅受热弹性阻尼而非支撑损失的限制。工艺引起的模式频移在挠性设计中得到有效补偿，以允许谐振频率在模式匹配操作的可调范围内。谐振模式的高频比低频 TFG 可以更有效地抵抗环境振动,并且器件的尺寸能够显着减小。虽然 X 和 Y 感测模式的灵敏度和噪声性能由于模式分离操作而不是最佳的,但该器件仍然能够执行偏置不稳定性的等级标准，以及 Z 感测模式的 ARW 和偏置不稳定性显示出模式匹配操作的改进。为了改进这种设计并减少稳定性偏差，必须在未来的工作中开发一种减少模式未对准影响的方案。由于该器件的刚度很大，正交抵消将需要更小的电容间隙（~200 nm 与 700 nm 相比），以便能够对结构施加大的力并确保高产量。

由于该器件的带宽允许非常大的满量程范围，因此可以在不牺牲大带宽优势的情况下增加 Q。未来的设备还将具有专为更高 Q 设计的弯曲部分，以确保设备仅受热弹性阻尼而非支撑损失的限制。

六、 致谢

作者要感谢 Haoran Wen 和 Mojtaba Hodjat Shamami 就陀螺仪设计和仿真进行了许多有价值的讨论。作者还希望感谢 DARPA MTO 对制造和测试的支持。

参考文献

[1] N. Yazdi,F. Ayazi,K. Najafi,“Micromachined Inertial Sensors,"Proc.IEEE, vol.86, no.8, pp.1640-1659,Aug 1998.

[2] M.F.Zaman,A. Sharma, Z.Hao, F. Ayazi,"A Mode-Matched Silicon-Yaw Tuning-Fork Gyroscope with Subdegree-Per-Hour Allan Deviation Bias Instability, "JMEMS, vol.17, no. 6, Dec 2008.

[3] H.Johari, F. Ayazi, "High-Frequency Capacitive Disk Gyroscopes in (100) and (111) Silicon,"Micro Electro Mechanical Systems Conference, pp. 47-50，21-25,Jan 2007.

[4] F. Ayazi,“Multi-DOF inertial MEMS: From gaming to dead reckoning, "Solid-State Sensors, Actuators and Microsystems Conference(TRANSDUCERS), Pp.2805-2808,June 2011.

[5] "Everything about STMicroelectronics’3-axis digital MEMS gyroscopes, "Technical Article TA0343, 2011

[6] G. Balachandran, V. Petkov, T. Mayer, T. Baislink,“A 3-Axis Gyroscope for Electronic Stability Control with Continuous Self-Test,” Solid-State Circuits Conference (ISSCC), pp.1-3, 22-26, Feb 2015.

[7] A. Partridge, M. Lutz,“Episeal Pressure Sensor and Method for Making an Episeal Pressure Sensor,'"U.S.Patent #6928879,Aug 16, 2005.

[8] R.N.Candler, M.A. Hopcroft, B. Kim, W.-T. Park, R. Melamud, M. Agarwal,G. Yama,A. Partridge, M.Lutz, and T.W. Kenny, "Long-Term and Accelerated Life Testing of a Novel Single-Wafer Vacuum Encapsulation for MEMS Resonators," JMEMS， Vol.15, No.6, pp. 1446-1456,2006.

[9] B. Kim, R.N.Candler,M.A. Hopcroft, M. Agarwal,W.-T. Park, and T. W. Kenny, "Frequency stability ofwafer-scale film encapsulated silicon based MEMS resonators, "Sensors and Actuators A: Physical, Vol.136, No. 1, pp.125-131,2007.

[10] M.S. Weinberg,A. Kourepenis, "Error Sources in In- Plane Silicon Tuning-Fork MEMS Gyroscopes,'"JMEMS, vol.15, no.3, pp. 479-491, June 2006.

[11] S.Sonmezoglu, P. Taheri-Tehrani, C. Valzasina, L.G. Falorni, S.Zerbini, S. Nitzan,D.A. Horsley,"Single-Structure Micromachined Three-Axis Gyroscope withReduced Drive-Force Coupling,”Electron DeviceLetters，IEEE, vol.36, no.9, pp. 953-956, Sept. 2015.

四、外文原文

IEEE Sensors Letters VOL. 2, NO. 4, DECEMBER 2018 2501404 IEEE Sensors Council

Mechanical sensors

A Quadruple Mass Vibrating MEMS Gyroscope With Symmetric Design

Guoqiang Wu, Geng Li Chua, Navab Singh, and Yuandong Gu
Institute of Microelectronics, Agency for Science, Technology and Research, Innovis, Singapore 138634

Manuscript received June 10, 2018; revised July 14, 2018 and August 7, 2018; accepted September 26, 2018. Date of publication October 1, 2018; date of current version October 15, 2018.

Abstract—This article presents a new microelectromechanical system (MEMS) quadruple mass gyroscope (QMG) with symmetric design. Similar to the wine-glass vibrating gyroscope, the reported QMG has a symmetric structure design both in the driving and sensing modes. The quadruple mass is coupled together using the central coupling springs and four tapered levers for the synchronization of the anti-phase driving motions. The reported QMG largely reduces the common mode signals due to accelerations and vibrations by the mechanical suppression. The momentum and torque balance in both driving and sensing directions contribute to ultra-low energy dissipation through the anchor, leading to a high quality factor (Q) and high resolution. The experimental measurement results show that the QMG demonstrates an Allan variance bias instability of 5.9°/h and a white noise level about 0.28°/$\sqrt{h}$, which are dominated by the flicker and thermal noise from the integrated circuit, respectively. The measured scale factor is 94.98 LSB/(°/s) with a nonlinearity of less than 600 ppm in the full-scale range of ±300°/s. The reported QMG demonstrates a new way to reach potential high-performance gyroscope designs for achieving high precision inertial measurement units.

Index Terms—Mechanical sensors, MEMS gyroscope, Coroilis effect, quadruple inertial masses, vibration insensitive, symmetric design.

I. INTRODUCTION

Microelectromechanical system (MEMS) gyroscopes have gained much attention in recent years, due to their small size, good performance, and high mass production capability [1]–[5]. MEMS gyroscopes already dominate the wide consumer markets, such as mobile phones, tablets, toys, gaming, and sports. However, higher performances are required in order to entre the high end automotive and industry applications, such as anti-roll and electronic stability control system for automotive, offshore navigation, stabilization systems, and drilling for industries.

Most of the MEMS gyroscopes are employing a linear or torsional vibrating structure to detect the external angular rate based on the Coriolis effect. One of the largest error sources for a vibrating MEMS gyroscope is the vibration sensitivity [6]. Mechanical vibrations in gyroscopes can create short-term output errors and degrade a device's performance. Therefore, a high rejection of environmental noise (vibration, acceleration, and shock) is essential for the reliable operation of a MEMS gyroscope. A differential sensor design with two anti-phase vibrating inertial masses can significantly reduce the vibration and acceleration induced errors. However, the faulty signals caused by the angular accelerations cannot be removed using the differential dual mass design [7]. In order to further improve the vibration rejection capability, a quadruple core MEMS gyroscope based on a dual differential design is proposed by Analog Devices Inc. [7]. A quadruple mass gyroscope (QMG) with four symmetrically decoupled tines is well developed by Shkel *et al.* [8]–[10], which provides an ultra-low energy dissipation and a high common mode acceleration rejection, as shown in Fig. 1(a). A center support quadruple mass gyroscope is reported and predicted to achieve good performance [11]. Bulk-acoustic wave gyroscopes also demonstrate high performance over the environmental stimuli, due to their inherent high stiffness and robustness [5]. Sagem has developed a novel vibrating gyroscope (Quapason) using a four beam metallic resonator. It has 3-D axisymmetric and shows very low sensitivity to external mechanical vibrations [12].

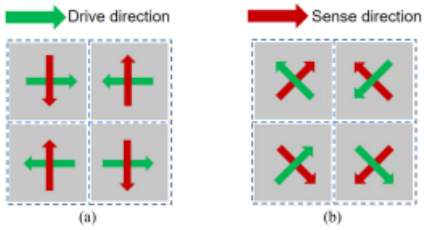

Fig. 1. Schematic illustration of two QMG designs. (a) Current QMG design: Two inertial masses in one column move close to each other, while the other two inertial masses in the other column move away from each other. (b) Proposed QMG design: Two inertial masses in one diagonal direction move away from each other, while the other two inertial masses in the other diagonal direction move close to each other.

In this article, we reported a new MEMS QMG with fully symmetric design, as shown in Fig. 1(b). It takes advantage of both the ideal symmetric design from the wine-glass gyroscope and the large inertial masses from the tuning fork gyroscopes. With the same operation mode shapes in [12], the QMG demonstrated here has the ideal symmetric design in both the driving and sensing directions. The momentum and torque balance in both the driving and sensing directions contributes to ultra-low energy dissipation through the anchor and results in a high rejection to external vibrations and shocks.

Corresponding author: Guoqiang Wu (e-mail: wugq@ime.a-star.edu.sg).
Associate Editor: A. M. Shkel.
Digital Object Identifier 10.1109/LSENS.2018.2873000

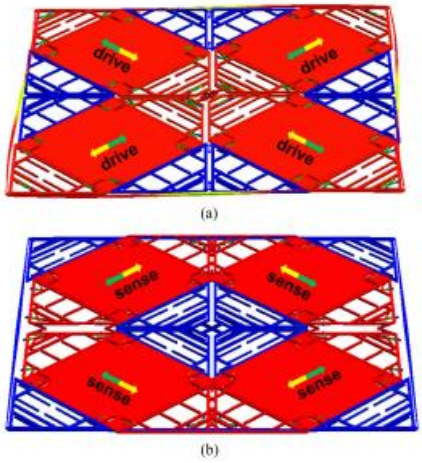

Fig. 2. Simulated mode shape deformations of the QMG. (a) Driving mode. (b) Sensing mode. The symmetric, anti-phase driving, and sensing modes result in complete dynamic balance, low energy dissipation, good anti-shock, and vibration rejection capability. Areas of red indicate the largest displacement occurring in the vibrating modes.

II. DESIGN AND OPERATION PRINCIPLES

Fig. 2 illustrates the simulated mode shape deformations of the reported QMG obtained by the finite element method using CoventorWare. Similar to the wine-glass gyroscope, the reported QMG has a symmetric design both in the driving and sensing modes. In the proposed design, the QMG consists of an outer frame and four inertial masses as an array comprising two rows and two columns within the outer frame. In the driving mode, two inertial masses in one diagonal direction move away from one another, while the other two inertial masses in the other diagonal direction move close to each other, as shown in Fig. 2(a). The quadruple inertial masses are coupled together using the central coupling springs and four tapered levers for the synchronization of the anti-phase driving motions. In the sensing mode, the two inertial masses in the first diagonal direction move away from each other in the direction perpendicular to the first diagonal line. The other two inertial masses in the second diagonal direction move away from each other in the direction perpendicular to the second diagonal line, as shown in Fig. 2(b). Comb fingers are used in the driving mode, and parallel plates are employed in the sensing mode. In this article, the mode split approach is adopted in order to achieve a large desired bandwidth. The simulated resonant frequencies of the driving mode and sensing mode are 13 961 Hz and 15 054 Hz, respectively. The simulated resonant frequency of the nearest undesired out-of-plane mode is 19 094 Hz.

An ideal symmetric design is achieved with this structure. The reported QMG design reduces the effects of the asymmetries of the sensor and has large rejection of the external vibrations and shocks. Moreover, the momentum and torque balance in both the driving and sensing directions contribute ultra-low energy dissipation through the anchor, leading to high quality factor (Q) and high resolution.

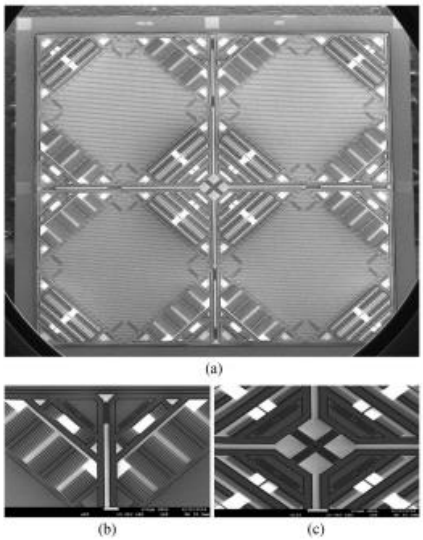

Fig. 3. SEM images of the fabricated QMG. (a) Overall view. The four inertial masses are coupled together with the outer frame and coupling springs. (b) Close-up view of the sense electrodes and the tapered lever. (c) Close-up view of the drive electrodes and the central coupling springs.

III. FABRICATION AND MEASUREMENT

The QMG is fabricated based on an 8-in silicon-on-insulator wafer with 30-μ m-thick device layer using a two mask process. The first mask defines the bonding pads, and the second mask forms the MEMS structures, followed by deep reactive ion etching (DRIE). Finally, the movable structures are released using vapor hydrogen fluoride dry etching. Fig. 3 shows the scanning electron microscope (SEM) images of the fabricated QMG. The four inertial masses and the coupling springs are clearly shown in Fig. 3. The measured width of the transduction gap is 1.2 μm. The measured average capacitances of the sense, drive, and monitor electrodes are 6.2 pF, 2.9 pF, and 2.8 pF, respectively. The size of the QMG is 5.8 mm $\times$ 5.8 mm $\times$ 0.7 mm (width $\times$ length $\times$ thickness).

After dicing, the QMG chip is vacuum encapsulated in a ceramic package to reduce the air damping [13]. The pressure inside the package carrier is less than 0.01 mbar [14]. The frequency response of the QMG is measured with a dynamic signal analyzer. The measured resonant frequencies of the driving mode and the sensing mode of the fabricated QMG are 12 940 Hz and 13 384 Hz, respectively. The measured frequencies are smaller than the simulation values (13 961 Hz and 15 054 Hz for driving mode and sensing mode, respectively), due to the critical dimension loss during the DRIE process. The measured Q value in the driving mode is 90 300 and in sensing mode is 39 200. The comb fingers used in the driving mode show a larger Q value since the dominating air damping mechanism is the slide damping, rather than the squeeze damping.

IEEE Sensors Letters VOL. 2, NO. 4, DECEMBER 2018 2501404

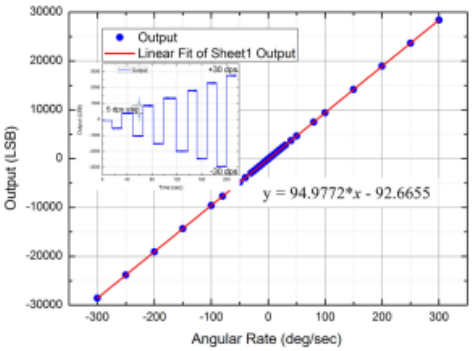

Fig. 4. Measured angular rate response of the QMG. The scale factor is measured as 94.98 LSB/(°/s.), and the scale factor nonlinearity is less than 600 ppm in the full-scale range of ±300°/s.

IV. GYRO SYSTEM MEASUREMENT

The packaged QMG is mounted on a printed circuit board to connect with a integrated circuit (IC). The reported QMG operates in the mode split approach, in which the sense resonant frequency is slightly larger than the drive resonant frequency to achieve a desired bandwidth [15]. The readout IC used in this article was purchased from TUMEMS technologies. It has the excitation and sensing electronics to obtain the angular rate characteristic of the MEMS gyroscope. The excitation loop uses a digital phase-locked loop to lock the movable drive frame and Coriolis frame vibrating in the drive resonant frequency. The movable structures maintain a constant drive amplitude by using an automatic gain control circuit. The sensing electronic extracts the rotation rate from the output of the sense electrodes by the differential low-noise charge amplifiers through the capacitor-to-voltage stage. After synchronous demodulation, a high resolution 16-bits analog-to-digital converter is employed to digitalize the output signals and output the detected angular rate to an I2C interface. The programmable band-pass filters are also included in the drive loop and sense loop in order to improve the signal to noise ratios.

A rate table is used to apply an angular rate to the QMG to get its angular rate response. Fig. 4 shows the measured angular rate response of the QMG. The input angular rate is from −300°/s to +300°/s. The digital output from the circuit is recorded with a I2C interface. The measured scale factor is 94.98 LSB/(°/s). The scale factor nonlinearity is less than 600 ppm in the full-scale range of ±300°/s. The measured response of the QMG system to both positive and negative input step of the angular rate rotations is shown in the inset of Fig. 4.

The zero rate output (ZRO) data are collected for 1.2 h at room temperature in order to evaluate the bias instability and angle random walk (ARW) of the MEMS gyroscope system. The root Allan variance curve of the gyroscope system is illustrated in Fig. 5. The inset is the time slice of the collected ZRO from the QMG system. The root Allan valiance curve indicates that the QMG shows a bias instability of 5.9°/h at an average time of around 10 s. The ARW of QMG is measured as 0.28°/√h, which is limited by the white noise from the electrical noise.

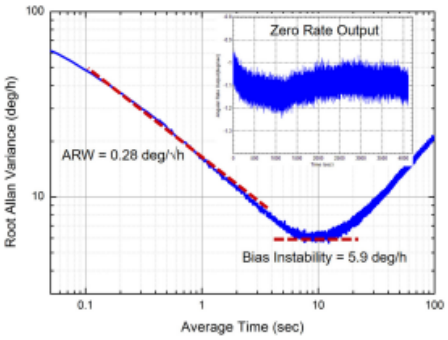

Fig. 5. Root Allan variance plot of the QMG system. A bias instability of 5.9°/h and a ARW of 0.28°/√h are obtained.

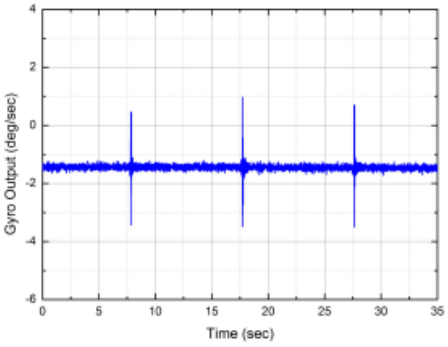

Fig. 6. Measured maximum bias shift of the QMG system under three half-sine shock acceleration signal with amplitude of 16 g and duration of 11 ms.

TABLE 1. Measured Parameters of the QMG System.

Parameters	Values	Units
Full scale range	±300	deg/sec
Scale factor	94.98	LSB/(deg/sec)
Scale factor non-linearity	600	ppm
Angle random walk	0.28	deg/√h
Bias instability	5.9	deg/h
Maximum bias shift under shock (amplitude: 16 g; duration: 11 ms)	4.5	deg/sec

The robustness of QMG with IC was verified by testing its reaction to the external shocks. The gyroscope system was fixed on the shaker. The shaker applies the half-sinusoidal shock acceleration signal along the z-axis of the QMG system. A total of three half-sinusoidal shaped excitation signals with amplitude of 16 g and 11-ms duration were applied at 10 s intervals. Fig. 6 shows the measured shock response of the QMG system. The maximum bias shift (peak to peak) of the QMG system is around 4.5°/s, possibly caused by the asymmetry of fabrication imperfection. Table 1 illustrates the measured parameters of the QMG system.

V. CONCLUSION

We reported a MEMS QMG with ideal symmetric design both in the driving mode and the sensing mode in this article. The quadruple masses are coupled together using the central coupling springs and four tapered levers for the synchronization of the anti-phase driving motions. The QMG is insensitive to external vibrations and shocks. The reported design paves the way for the silicon-based vibrating MEMS gyroscope entering into high-end inertial navigation applications.

REFERENCES

[1] K. Liu *et al.*, "The devel-opment of micro-gyroscope technology," *J. Micromech. Microeng.*, vol. 19, no. 11, Oct. 2009, Art. no. 113001.

[2] F. Ayazi and K. Najafi, "A HARPSS polysilicon vibrating ring gyroscope," *J. Microelectromech. Syst.* vol. 10, no. 2, pp. 169–179, Jun. 2001.

[3] S. E. Alper, Y. Temiz, and T. Akin, "A compact angular rate sensor system using a fully decoupled silicon-on-glass MEMS gyroscope," *J. Microelectromech. Syst.*, vol. 17, no. 6, pp. 1418–1429, Dec. 2008.

[4] S. Sonmezoglu *et al.*, "Single-structure micromachined 3-axis gyroscope with reduced drive-force coupling," *IEEE Electron Device Lett.*, vol. 36, no. 9, pp. 953–956, Sep. 2015.

[5] D. E. Serrano *et al.*, "Substrate-decoupled, bulk-acoustic wave gyroscopes: Design and evaluation of next-generation environmentally robust devices," *Microsyst. Nanoeng.*, vol. 2, Feb. 2016, Art. no. 16015.

[6] H. Weinberg, "Gyro mechanical performance: The most important parameter," Tech. Art., Analog Devices, Norwood, MA, USA, Sep. 2011. [Online]. Aviliable: http://www.analog.com/media/en/technical-documentation/tech-articles/MS-2158.pdf

[7] M. Füldner, "Vibration-immune multi-core MEMS gyroscopes are improving auto safety," Analog Devices, Norwood, MA, USA.

[8] A. Trusov, I. Prikhodko, S. Zotov, and A. Shkel, "Low-dissipation silicon tuning fork gyroscopes for rate and whole angle measurements," *IEEE Sens. J.*, vol. 11, no. 11, pp. 2763–2770, Nov. 2011.

[9] A. A. Trusov *et al.*, "Flat is not dead: Current and future performance of Si-MEMS quad mass gyro (QMG) system," in *Proc. IEEE/ION Position Location Navigat. Symp.*, May 2014, pp. 252–258.

[10] S. A. Zotov, A. A. Trusov, and A. M. Shkel, "High-range angular rate sensor based on mechanical frequency modulation," *J. Microelectromech. Syst.*, vol. 21, no. 2, pp. 398–405, Apr. 2012.

[11] B. Zhou, T. Zhang, P. Yin, Z. Y. Chen, M. L. Song, and R. Zhang, "Innovation of flat gyro: Center support quadruple mass gyroscope," in *Proc. IEEE Int. Symp. Inertial Sens. Syst.*, Laguna Beach, CA, USA, Feb. 22–25, 2016, pp. 1–4.

[12] P. Leger, "Quapason^{TM}—A new low-cost vibrating gyroscope," in *Proc. 3rd St. Petersburg Int. Conf. Integr. Navigat. Syst.*, Saint Petersburg, Russia, May 1996, p. 15.

[13] M. H. Asadian, S. Askari, and A. M. Shkel, "An ultra-high vacuum packaging process demonstrating over 2 million Q-factor in MEMS vibratory gyroscopes," *IEEE Sens. Lett.*, vol. 1, no. 6, Dec. 2017, Art. no. 6500104.

[14] G. Q. Wu, D. H. Xu, B. Xiong, L. F. Che, and Y. L. Wang, "Design, fabrication and characterization of a resonant magnetic field sensor based on mechanically coupled dual-microresonator," *Sens. Actuators A: Phys.*, vol. 248, pp. 1–5, Sep. 2016.

[15] G. Q. Wu, G. L. Chua, and Y. D. Gu, "A dual-mass fully decoupled MEMS gyroscope with wide bandwidth and high linearity," *Sens. Actuators A: Phys.*, vol. 259, pp. 50–56, Mar. 2017.

A HIGH-FREQUENCY EPITAXIALLY ENCAPSULATED SINGLE-DRIVE QUAD-MASS TRI-AXIAL RESONANT TUNING FORK GYROSCOPE

S. Wisher[1], P. Shao[1], A. Norouzpour-Shirazi[1], Y. Yang[2], E. Ng[2], I. Flader[2], Y. Chen[2], D. Heinz[2], T. Kenny[2], and F. Ayazi[1]

[1]Georgia Institute of Technology, Atlanta, GA, USA

[2]Stanford University, Palo Alto, CA, USA

ABSTRACT

This paper introduces a 'high-frequency' resonant tri-axial tuning fork gyroscope (TFG) with a single-drive mode of operation. The quad-mass device is implemented on a 2x2 mm^2 vacuum-packaged die fabricated using the *epi-seal* process, making this one of the smallest wafer-level packaged 3-axis gyros. In contrast to conventional resonant TFGs, the resonant frequencies are designed to be relatively high (~138 kHz) permitting high bandwidth for mode-matched operation and enhancing resistance to shock and vibration. The results show sensitivity to all three axes with mode-matched operation for the Z-axis and mode-split for the X- and Y- axes.

INTRODUCTION

Micromachined gyroscopes are widely used in many applications ranging from automotive safety to image stabilization for cameras, with the range of applications expanding as the MEMS gyroscope technology advances. The most common type of MEMS gyroscope designs is the TFG, a shuttling proof mass design that can be operated at either mode-matched or mode-split condition. While mode-split operation allows for a very wide, adjustable dynamic range and relatively good scale factor stability across temperature, its applications are limited by the poor signal-to-noise performance. Mode-matched operation can significantly boost the mechanical signal-to-noise ratio (SNR) through Q amplification, but the primary limitation of high-Q, mode-matched gyroscopes is the reduced dynamic range due to small open-loop mechanical bandwidth. By increasing the operation frequency of mode-matched resonant gyroscopes, the mechanical bandwidth can be increased [1]-[3].

The multiple degree-of-freedom (DOF) inertial measurement units (IMU) can be used on platforms to boost GPS performance and, in some cases, eliminate the need for GPS entirely. Multiple solutions have been presented to implement 3-axis gyroscopes for use in multi-DOF IMU. Traditionally, three individual single-axis gyroscope dies have been oriented to detect rotation about each axis. This technique, while providing very high performance for all the axes, requires sophisticated packaging techniques to minimize axis misalignment while also demanding a larger and thicker package to house the 3D-arranged devices. Another common solution is to implement three gyroscopes on a common die [4], presenting an effective solution for cost sensitive, less stringent applications in a small package size. Among these, designs that utilize a single-drive mechanism to sense X, Y, and Z rotations simultaneously usually provide the lowest power. STMicroelectronics and Bosch have both developed devices based on this concept [5], [6]. However, these designs are all at low frequency and are subject to limitations for operation in mode-matched condition, along with susceptibility to shock and vibration.

The device presented in this paper is the first attempt to increase the modal frequencies of a moving-mass resonant TFG to much higher than that of conventional TFGs for increased bandwidth and dynamic range, along with improved resistance to shock and linear vibration. Additionally, gyroscope operation is expanded to three axes with a single-drive mechanism.

HIGH-FREQUENCY TRI-AXIAL TFG

The presented device consists of four proof masses that are connected to anchors by "fishhook" flexures to support both in-plane and out-of-plane motion. Fig. 1 shows the device geometry, and Fig. 2 shows the COMSOL eigenfrequency simulation plots of the drive and sense resonant modes of the device in which the four proof masses of the device are driven into motion by a center electrode. When subjected to rotation, energy is transferred between the drive mode and the gyroscopic sense modes through Coriolis coupling.

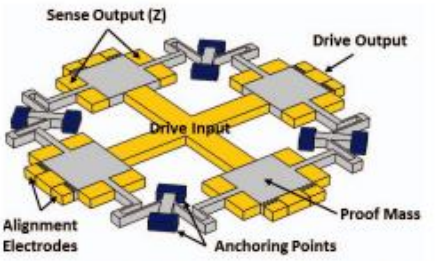

Figure 1: Schematic of the single-drive quad-mass tri-axial TFG, illustrating electrodes and anchoring points.

In contrast to conventional resonant TFGs, this device was designed to have relatively high resonant frequencies (~138 kHz) to improve the device bandwidth under mode-matched conditions and to enhance the robustness to shock and vibration. With an external linear vibration, the device can exhibit translational motion, and in some cases, these external vibrations are caused by sonic disturbances with frequencies in the range of 10-20 kHz, which is also the range of frequencies for conventional resonant TFGs. These translational modes typically have resonant frequencies close to that of the sense and drive modes in such TFGs. With disturbances close to the frequencies of resonant modes, the instability of the sense output significantly increases, and it can be shown that by

978-1-5090-1973-1/16/$31.00 ©2016 IEEE

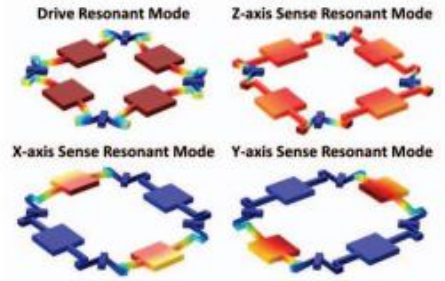

Figure 2: Drive mode, Z-axis sense mode, X-axis sense mode, and Y-axis sense mode shape plots generated by COMSOL.

increasing the TFG resonant frequencies to much higher than that of external vibration, the sensitivity to external vibration can be dramatically reduced.

An additional benefit of a higher frequency device is the reduced size of high-frequency TFG designs due to smaller dimensions of flexures and proof masses; however, the reduced flexure dimensions cause the resonant frequencies to shift more sharply due to process imperfections such as sidewall tilt. When designing the modes to be within tunable range of each other, these considerations are especially important since the dimensions of the flexures corresponding to each resonant mode differ. Modal resonant frequency shifts are seen due to sidewall tilt. With a characterized, repeatable process, these frequency shifts can be compensated in the design of the flexures.

While most TFGs use comb-drive electrodes for actuation, the increased stiffness of this device is more effectively actuated by parallel-plate electrodes, which more easily apply larger drive forces and allow for a sensitive current output. Sense mode frequencies were designed to be higher than the drive mode, and the electrode design utilizes different capacitive gap dimensions for the drive and sense electrodes to reduce the Z-axis sense mode frequency much more steeply than that of the drive, X, and Y modes through electrostatic spring softening by increasing the polarization voltage (V_P). This design allows for the Z mode to be matched to the drive mode. The X and Y modes are also tuned by increasing V_P, but to further enhance the flexibility of the electrostatic tuning, voltage can be applied to the dedicated top electrodes, which border the out-of-plane sense electrodes. The resonant frequencies of approximately 138 kHz were chosen to allow the device to be compliant enough for the tuning of the drive and sense modes while still being high enough to effectively reject vibrations and increase bandwidth. Alignment electrodes were also included to reduce the in-plane mode misalignment, but to increase their effect, larger forces must be applied to entirely cancel this effect. Due to the strong relationship between electrostatic force and gap size, the effectiveness of the alignment electrodes in this presented work will need to have reduced capacitive gap sizes to improve upon the robustness of this design.

FABRICATION AND PACKAGING

The device was fabricated and wafer-level packaged using the *epi-seal* process developed by researchers at Stanford University and Bosch RTC [7-8]. The process starts with an SOI wafer with 40 µm device layer and 2 µm buried oxide layer. The resonator outline is defined by etching trenches in the device layer using deep-reactive-ion etching (DRIE). Next, a sacrificial oxide layer is deposited to form an oxide spacer layer above the device. Contacts are then etched in the oxide layer, followed by deposition of the 1st silicon layer. Nitride plugs are formed to define top electrode outline. Vent holes are then etched into the silicon cap, and vapor HF is used to release the resonating structures. Immediately after the release, devices are sealed in an epitaxial reactor chamber by depositing a final layer of silicon. Lastly, electrical isolation and metal contacts are defined. This process provides a clean, low-pressure operating environment, which allows the devices to achieve long-term stability operations [9]. A cross-section diagram highlighting the layers of the process are shown in Fig. 3, and an SEM of the presented TFG design is shown in Fig. 4.

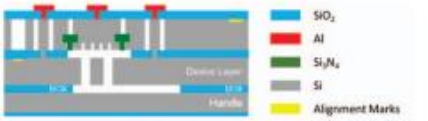

Figure 3: Cross-section illustrating the various layers of a device fabricated through the epi-seal process.

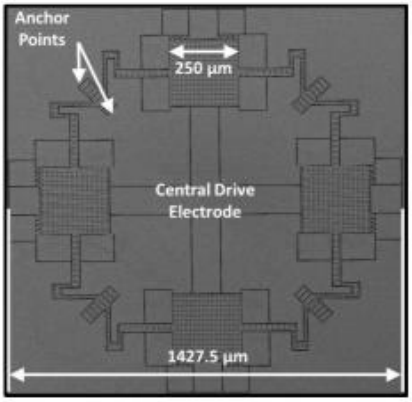

Figure 4: Top SEM view of the single-drive tri-axial TFG fabricated and packaged through the epi-seal process.

EXPERIMENTAL RESULTS

The results were obtained by using a Zurich Instruments HF2LI lock-in amplifier with the TFG bonded to the custom PCB shown in Fig. 5. The output current of each sense mode was given to a trans-impedance amplifier (TIA) to amplify the rate signal and convert it to a voltage. The drive and Z modes were matched when a V_P of 47.9 V was applied. Fig. 6 shows the resonant frequencies

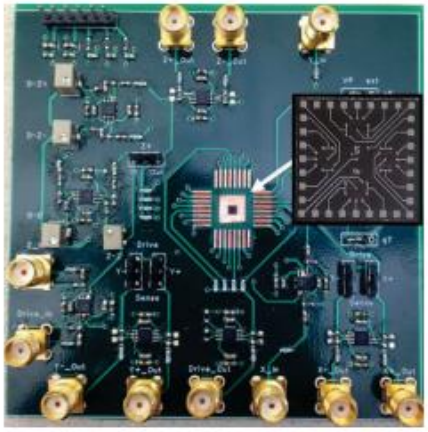

Figure 5: Custom gyroscope-interfacing PCB that includes buffers, TIAs, and feedthrough cancellation circuits to be used in conjunction with a lock-in amplifier, and the wafer-level-packaged tri-axial TFG die.

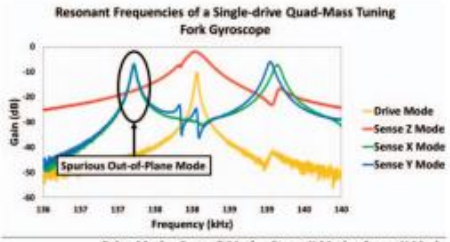

	Drive Mode	Sense Z Mode	Sense X Mode	Sense Y Mode
Frequency (Hz)	138058	138043	139140	139048
Quality Factor	3910	505.0	1181	1360
Bandwidth (Hz)	35.0	273	118	102

Figure 6: Characterization data showing the various drive and sense mode peak values under mode-matched condition for Z-sense and mode-split for X- and Y-sense.

of the device after tuning, and the Z mode frequency was electrostatically matched with that of the drive mode. The X and Y modes are able to be tuned to the level of the drive and sense modes by means of the top tuning electrodes, but by applying 43 V and 21 V to the X and Y tuning electrodes, respectively, they were tuned to frequencies of approximately 1 kHz higher to minimize cross-coupling effects between out-of-plane and in-plane modes. This frequency split was chosen to allow the drive and Z modes to fall between the X and Y modes and an out-of-plane spurious mode to reduce the mode coupling between the in-plane and out-of-plane modes as much as possible. Fig. 7 shows the sensitivity plots of the output current in response to rotation. The mode-matched Z-axis sensitivity is 30.5 pA/°/s, and the sensitivities of the mode-split X and Y axes are 1.40 pA/°/s and 1.21 pA/°/s, respectively. In this case, sensitivity is reduced by capacitive gap size limitations and mode misalignment. Since the X and Y modes cannot be

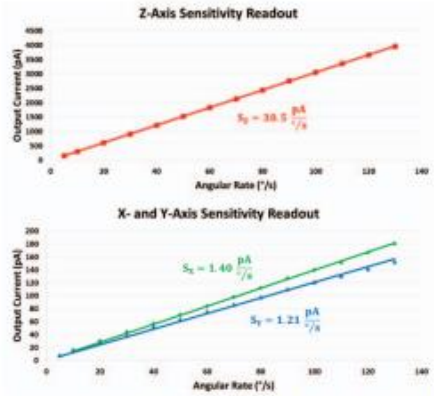

Figure 7: Sensitivity plots showing the output current (pA) relationship to angular rate (°/s) about the Z, X, and Y axes.

matched to drive due to modal cross-coupling, future improvements will require an out-of-plane cross-coupling cancellation scheme between the in-plane and out-of-plane modes to allow for the matching of the X and Y modes to that of the drive mode. With a fully mode-matched tri-axial TFG design, X- and Y- axis sensitivity can be significantly improved.

Allan variance data was collected to evaluate the noise performance for each axis of rotation, and the information is shown in Fig. 8. The angle random walk (ARW) represents the white noise of the system as rotation, and the bias instability represents the best achievable drift of bias. The mode-matched Z-axis noise performed similarly to a 3-axis gyroscope presented in [10], in which the authors reach an ARW of 0.039 °/√s and a bias instability of 0.042 °/s for the Z-axis after the reduction of drive-force coupling. Drive-force coupling and quadrature coupling are both results of mode misalignment due to fabrication imperfections, and they result in the increase of bias error [11]. Quadrature coupling is typically much higher than

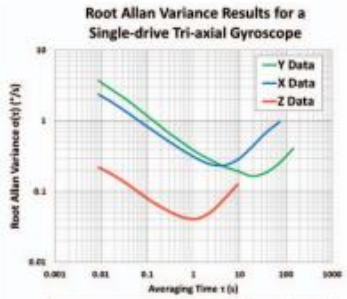

	X-axis	Y-axis	Z-axis
Angle Random Walk (°/√s)	0.292	0.357	0.028
Bias Instability (°/s)	0.226	0.166	0.041

Figure 8: Root Allan variance plot showing the ARW and bias instability for each output of the tri-axial TFG.

that of the rate signal, and without a means for quadrature decoupling, any small shift in the demodulation phase of the readout circuits will cause a noticeable shift in bias. Therefore, to improve upon the bias performance of the presented device, the quadrature cancellation must be enhanced.

The high-frequency design of the TFG shows the bandwidth of the Z mode to be in excess of 100 Hz. The operating frequencies of the tuned drive and sense modes range from 138.043 kHz to 139.140 kHz. Increased frequencies of operation gives this gyroscope the necessary properties to reject environmental sonic and ultrasonic disturbances which often occur at much lower frequencies.

CONCLUSION

This work presents a high-frequency single-drive quad-mass TFG that shows rate sensitivity about all three axes of rotation, implemented on a 2x2 mm^2 wafer-level packaged die. Process-induced frequency shifts of the modes were effectively compensated in the flexure designs to allow the resonant frequencies to be within the tunable range for mode-matched operation. The high frequencies of the resonant modes can more effectively resist environmental vibration than low-frequency TFGs, and the size of the device is able to be significantly reduced. While the sensitivity and noise performance of the X and Y sense modes were not optimal due to mode-split operation, the device was still able to perform to rate-grade standards for bias instability, and the ARW and bias instability of the Z sense mode showed improvement with mode-matched operation. To improve upon this design and reduce the bias instability, a scheme to reduce the effects of mode misalignment must be developed in future work. Due to the large stiffness of this device, the quadrature cancellation will require smaller capacitive gaps (~200 nm compared to 700 nm) to have the ability to apply large forces to the structure and ensure a high yield.

Since the bandwidth of this device allows for a very large full-scale range, the Q can be increased without sacrificing the benefits of a large bandwidth. Future devices will also have flexures that are designed for higher Qs to ensure that the device is solely limited by thermoelastic damping rather than support loss.

ACKNOWLEDGEMENTS

The authors wish to thank Haoran Wen and Mojtaba Hodjat-Shamami for many valuable discussions on gyroscope design and simulation. The authors also wish to thank support from DARPA MTO for fabrication and testing.

REFERENCES

[1] N. Yazdi, F. Ayazi, K. Najafi, "Micromachined Inertial Sensors," *Proc. IEEE*, vol. 86, no. 8, pp. 1640-1659, Aug 1998.

[2] M.F. Zaman, A. Sharma, Z. Hao, F. Ayazi, "A Mode-Matched Silicon-Yaw Tuning-Fork Gyroscope with Subdegree-Per-Hour Allan Deviation Bias Instability," *JMEMS*, vol. 17, no. 6, Dec 2008.

[3] H. Johari, F. Ayazi, "High-Frequency Capacitive Disk Gyroscopes in (100) and (111) Silicon," *Micro Electro Mechanical Systems Conference, pp. 47-50, 21-25, Jan 2007.*

[4] F. Ayazi, "Multi-DOF inertial MEMS: From gaming to dead reckoning," *Solid-State Sensors, Actuators and Microsystems Conference (TRANSDUCERS)*, pp. 2805-2808, June 2011.

[5] "Everything about STMicroelectronics' 3-axis digital MEMS gyroscopes," Technical Article TA0343, 2011

[6] G. Balachandran, V. Petkov, T. Mayer, T. Baislink, "A 3-Axis Gyroscope for Electronic Stability Control with Continuous Self-Test," *Solid-State Circuits Conference (ISSCC)*, pp. 1-3, 22-26, Feb 2015.

[7] A. Partridge, M. Lutz, "Episeal Pressure Sensor and Method for Making an Episeal Pressure Sensor," U.S. Patent #6928879, Aug 16, 2005.

[8] R. N. Candler, M. A. Hopcroft, B. Kim, W.-T. Park, R. Melamud, M. Agarwal, G. Yama, A. Partridge, M. Lutz, and T. W. Kenny, "Long-Term and Accelerated Life Testing of a Novel Single-Wafer Vacuum Encapsulation for MEMS Resonators," *JMEMS*, Vol. 15, No. 6, pp. 1446-1456, 2006.

[9] B. Kim, R. N. Candler, M. A. Hopcroft, M. Agarwal, W.-T. Park, and T. W. Kenny, "Frequency stability of wafer-scale film encapsulated silicon based MEMS resonators," *Sensors and Actuators A: Physical*, Vol. 136, No. 1, pp. 125-131, 2007.

[10] M.S. Weinberg, A. Kourepenis, "Error Sources in In-Plane Silicon Tuning-Fork MEMS Gyroscopes," *JMEMS*, vol. 15, no. 3, pp. 479-491, June 2006.

[11] S. Sonmezoglu, P. Taheri-Tehrani, C. Valzasina, L.G. Falorni, S. Zerbini, S. Nitzan, D.A. Horsley, "Single-Structure Micromachined Three-Axis Gyroscope with Reduced Drive-Force Coupling," *Electron Device Letters, IEEE*, vol. 36, no. 9, pp. 953-956, Sept. 2015.

CONTACT

S. P. Wisher, tel: +1-318-2285170;
swisher3@gatech.edu

毕业论文（设计）文献综述和开题报告考核

对文献综述、外文翻译和开题报告评语及成绩评定

成绩比例	文献综述 占（10%）	开题报告 占（15%）	外文翻译 占（5%）
分值			

开题报告答辩小组负责人（签名）_____

年　　月　　日